

1  
2  
3  
4  
5  
6  
7  
8  
9  
10  
11  
12  
13  
14  
15  
16  
17  
18  
19  
20  
21

## Neural crest cells bulldoze through the microenvironment

### using Aquaporin-1 to stabilize filopodia

Rebecca McLennan<sup>1</sup>, Mary C. McKinney<sup>1</sup>, Jessica M. Teddy<sup>1</sup>, Jason A. Morrison<sup>1</sup>, Jennifer C. Kasemeier-Kulesa<sup>1</sup>, Dennis A. Ridenour<sup>1</sup>, Craig A. Manthe<sup>1</sup>, Rasa Giniunaite<sup>2</sup>, Martin Robinson<sup>2,4</sup>, Ruth E. Baker<sup>2</sup>, Philip K. Maini<sup>2</sup>, Paul M. Kulesa<sup>1,3,\*</sup>

1. Stowers Institute for Medical Research, Kansas City, MO, 64110, USA.
2. Oxford University, Wolfson Centre for Mathematical Biology, Woodstock Road, Oxford, OX2 6GG, UK
3. Department of Anatomy and Cell Biology, University of Kansas School of Medicine, Kansas City, KS, 66160, USA
4. Oxford Centre for Collaborative Applied Mathematics, Mathematical Institute, 24-29 St Giles', Oxford OX1 3LB, UK

\*corresponding author: [pmk@stowers.org](mailto:pmk@stowers.org)

**26 July, 2019**

1 **ABSTRACT**

2 Neural crest migration requires cells to move through an environment filled with dense  
3 extracellular matrix and mesoderm to reach targets throughout the vertebrate embryo.

4 Here, we use high-resolution microscopy, computational modeling, and in vitro and in  
5 vivo cell invasion assays to investigate the function of Aquaporin-1 (AQP-1) signaling.

6 We find that migrating lead cranial neural crest cells express AQP-1 mRNA and protein,  
7 implicating a biological role for water channel protein function during invasion.

8 Differential AQP-1 levels affect neural crest cell speed, direction, and the length and  
9 stability of cell filopodia. Further, AQP-1 enhances matrix metalloprotease (MMP)  
10 activity and colocalizes with phosphorylated focal adhesion kinases (pFAK). Co-  
11 localization of AQP-1 expression with EphB guidance receptors in the same migrating  
12 neural crest cells raises novel implications for the concept of guided bulldozing by lead  
13 cells during migration.

14

15

## 1 INTRODUCTION

2 Cell migration is essential during embryogenesis to gastrulate, elongate the vertebrate  
3 axis, and distribute cells into the periphery to contribute to organ development. Despite  
4 the importance of cell migration to human development and disease, it is still unclear  
5 what mechanisms enable cells to invade the dense ECM, mesoderm and other cell  
6 types characteristic of the embryonic microenvironment. The complexity of the  
7 embryonic microenvironment means that invading cells must rapidly change cell shape  
8 and volume, form and sustain protrusions that penetrate different sized gaps, and attach  
9 to and remodel the ECM. Thus, there is a tremendous need to identify and test the  
10 function of molecules critical to embryonic cell migration and better understand their  
11 mechanistic basis.

12

13 Neural crest cell migration is one of the most prevalent examples of how cells efficiently  
14 distribute throughout the growing vertebrate embryo to precise targets. In the head,  
15 cranial neural crest cells must invade through dense ECM, loosely connected  
16 mesoderm, and migrating endothelial cells. Yet, it has remained unclear how the  
17 migrating neural crest cells that first encounter the embryonic microenvironment  
18 penetrate small gaps between mesodermal cells and degrade the ECM to move in a  
19 directed manner to peripheral targets. By combining dynamic in vivo imaging and super  
20 resolution microscopy with gain- and loss-of-function experiments, we are poised to  
21 examine the function of genes presumed critical to neural crest cell migration. Thus, the  
22 embryonic neural crest is an attractive in vivo model to study the function of cell  
23 invasion genes in mechanistic detail.

1 Using single cell RT-qPCR and transcriptome profiling, we discovered the enhanced  
2 expression of several genes in the most invasive chick cranial neural crest cells,  
3 including *AQP-1* (McLennan et al., 2015a; Morrison et al., 2017a). *AQP-1* is a  
4 transmembrane channel protein that facilitates the flux of water across the plasma  
5 membrane (Agre et al., 1993) and is one member of a family of at least 13 aquaporins  
6 (Ishibashi et al., 2011). *AQP-1* has been detected in several aggressive human cancers  
7 and its expression correlates with poor disease prognosis (Tomita et al., 2017; De Ieso  
8 and Yool, 2018). However, the mechanistic basis of *AQP-1* function is still unclear since  
9 studies have been limited to analyzing cell behaviors using in vitro assays. This has led  
10 to the generation of several distinct hypothetical mechanisms of *AQP-1* function. For  
11 example, *AQP-1* is thought to allow cells to rapidly change cell volume to form thin  
12 filopodial protrusions that squeeze in between neighboring cells (Papadopoulos et al.,  
13 2008; Verkman, 2009; Karlsson et al., 2013) or collapse a cell protrusion to retreat from  
14 a repulsive signal (Cowan et al., 2000). Alternatively, *AQP-1* may function to stabilize a  
15 filopodium since aquaporins have been shown in vitro to localize to the front end of  
16 migrating cells (Saadoun et al., 2005) and are speculated to function as a cell motility  
17 engine (Condeelis, 1993; Stroka et al., 2014). Thus, a better understanding of the in  
18 vivo function of *AQP-1* and its connection to cell guidance signaling would be beneficial  
19 to studies in cell migration and invasion in cancer and developmental biology.

20

21 In this study, we examined the expression and function of *AQP-1* during chick cranial  
22 neural crest cell migration and possible upstream guidance and downstream *AQP-1*

1 effectors. We first characterized *AQP-1* mRNA and AQP-1 protein expression within  
2 migrating cranial neural crest cells using 3D confocal and super resolution microscopy.  
3 We examined the role of AQP-1 in vitro and in vivo by measuring changes to the neural  
4 crest cell migratory pattern, individual cell behaviors, and filopodial dynamics after gain-  
5 and loss-of-function of AQP-1. To test our hypothesis of a “bulldozer” role for AQP-1  
6 expressing neural crest cells, we analyzed focal adhesion activity, integrin localization  
7 and ECM degradation after AQP-1 manipulation. We examined the possible co-  
8 localization of Eph guidance receptor expression with AQP-1 in the same migrating  
9 neural crest cells using multiplexed fluorescence in situ hybridization. Lastly, we use  
10 computer simulations to predict what AQP-1 related functions are likely to enhance cell  
11 migration. Together, our data demonstrate a critical role for AQP-1 during cranial neural  
12 crest cell migration and offer a mechanistic basis for in vivo AQP-1 function to promote  
13 cell invasion.

14

15

## 1 RESULTS

### 2 ***Aquaporin-1* mRNA is expressed in migrating cranial neural crest cells and** 3 **preferentially within the lead subpopulation**

4 To detect the expression of *AQP-1* mRNA in vivo specifically within migrating cranial  
5 neural crest cells, we took advantage of our recently optimized integrated protocol  
6 combining RNAscope multiplexed fluorescence in situ hybridization,  
7 immunohistochemistry (IHC), and tissue clearing with FRUIT (Morrison et al., 2017b).  
8 This enabled the detection of *AQP-1* mRNA expression in migrating HNK-1 labeled  
9 neural crest cells (Fig. 1A-C). By spot counting the number of *AQP-1* transcripts per  
10 neural crest cell, we found that *AQP-1* expression was visible in migrating cranial neural  
11 crest cells observed at Hamburger and Hamilton stage (HH) 13 (Hamburger and  
12 Hamilton, 1951) enroute from rhombomere 4 (r4) to the second branchial arch (BA2)  
13 (Fig. 1C; neural crest cells are color-coded to show number of *AQP-1* counted  
14 transcripts). In a typical r4 neural crest cell migratory stream, the highest numbers of  
15 detected transcripts of *AQP-1* were found to be in the cell subpopulation at the front of  
16 the migratory stream (Fig. 1C). We determined this by quantifying the fluorescence  
17 signal of *AQP-1* mRNA expression as a function of distance along the migratory stream  
18 (from the neural tube towards BA2) in a large number of cells/embryos (Fig. 1D). This  
19 confirmed that lead neural crest cells showed significantly higher level of *AQP-1*  
20 expression compared to cells further back in the invading stream (Fig. 1D).

21

22

1 **Aquaporin-1 protein is localized on the cell membrane of neural crest cells,**  
2 **including filopodia in vitro and expressed throughout the migratory stream in**  
3 **vivo**

4 Whether AQP-1 protein is expressed within subregions of individual migrating neural  
5 crest cells is difficult to determine since it is challenging to resolve fluorescence signal in  
6 thin (1-2 um wide) protrusions. Structured illumination microscopy (SIM) has emerged  
7 as an excellent tool to resolve diffraction limited issues by increasing optical resolution  
8 (Gustafsson et al., 2008). When we applied SIM to visualize AQP-1 protein location  
9 within migrating neural crest cells in vitro, we discovered AQP-1 was present on the cell  
10 membranes including the tips of filopodia (Fig. 1E). To determine AQP-1 protein  
11 expression in vivo, we analyzed AQP-1 protein by IHC within HNK-1 labeled migrating  
12 neural crest cells and confirmed AQP-1 expression throughout the migratory stream  
13 (Fig. 1F, G; HH11-15). Further, by quantifying fluorescent intensity in individual leader  
14 and follower neural crest cells, we determined that there is a higher level of AQP-1  
15 protein in the lead neural crest cells in vivo (Fig. 1H). These data suggested that AQP-1  
16 may be influencing the formation, stability and/or the retraction of neural crest cell  
17 filopodia at the leading edge of the migratory stream.

18

19 **Aquaporin-1 perturbations in vitro alter neural crest cell speed**

20 To begin to determine the function of AQP-1 in cranial neural crest cell migration, we  
21 explanted cranial neural tubes in an in vitro assay and measured changes in cell  
22 migratory behaviors with confocal time-lapse microscopy (Fig. 2A, B). We took

1 advantage of Acetazolamide (AZA), a chemical inhibitor of AQP-1 function (Bin and Shi-  
2 Peng, 2011; Zhang et al., 2012; Cai et al., 2018; Ameli et al., 2012). Although AZA can  
3 also affect AQP-4 function, AQP-1 is the only aquaporin significantly expressed by the  
4 invasive front of the migratory stream and therefore the only aquaporin significantly  
5 affected by AZA in this assay (Huber et al., 2007; McLennan et al., 2015a; Morrison et  
6 al., 2017a). When we inhibited AQP-1 function in vitro, we observed that the migrating  
7 neural crest cells moved significantly slower than control neural crest cells (in the  
8 presence of DMSO) (Fig. 2B, C; Supplemental Movie 1). Representative tracks show  
9 that neural crest cells exposed to AZA remained closer to the neural tube explant and  
10 other cells than controls (Fig. 2E).

11

12 To determine changes in cell migration after AQP-1 gain-of-function, we over-expressed  
13 AQP-1 in premigratory neural crest cells (by transfection with AQP-1 FL) and again  
14 explanted neural tubes in culture (Fig. 2A, B). AQP-1 over-expression resulted in neural  
15 crest cells that moved significantly faster when compared to non-transfected cells in the  
16 same culture (Fig. 2B, C; Supplemental Movie 1). Neural crest cells overexpressing  
17 AQP-1 were also significantly faster when compared to EGFP only (pMES) transfected  
18 cells from different cultures that were prepared and imaged concurrently (Supplemental  
19 Fig. 1D). Typical cell tracks from gain-of-function of AQP-1 experiments confirmed  
20 neural crest cells moved further away from the neural tube explant in the same amount  
21 of time (Fig. 2F). Interestingly, when AQP-1 was overexpressed, cells migrated with  
22 increased straightness compared to their controls (Fig. 2D). These in vitro data



1 suggested that AQP-1 significantly influences the speed at which neural crest cells  
2 migrate.

3

#### 4 **Inhibition of Aquaporin-1 in vivo results in fewer neural crest cells invading** 5 **branchial arch 2**

6 To determine the in vivo function of AQP-1, we first knocked down AQP-1 function in  
7 premigratory cranial neural crest cells by morpholino (MO) transfection. Similar to in  
8 vitro experiments, AQP-1 MO transfected neural crest cells did not travel as far as in  
9 control MO transfected neural crest cells (Fig. 3A, C, D). In AQP-1 MO transfected  
10 embryos, we found fewer migrating transfected neural crest cells in BA2 compared to  
11 control MO transfected embryos (Fig. 3B). To further verify the in vivo loss of AQP-1  
12 function in neural crest cell migration, we microinjected AZA into the paraxial mesoderm  
13 adjacent to r4, prior to neural crest cell exit from the dorsal neural tube. AZA injected  
14 sides of embryos showed fewer migrating neural crest cells migrating into BA2  
15 compared to control sides of the same embryos (Fig. 3F) and control DMSO injected  
16 embryos, as seen with immunolabeling of neural crest cells using HNK-1 (Fig. 3G). We  
17 also measured fewer neural crest cells present in BA2 when injected with AZA as  
18 quantified by percentage of HNK-1 immunostaining signal in BA2 (Fig. 3E). The furthest  
19 distance migrated after AZA injection was the same as control, either due to cells  
20 escaping AZA, dilution/degradation of the AZA over time or differences in how AZA  
21 versus a morpholino affect AQP-1 activity (Supplemental Fig. 1E). There was no  
22 significant difference of HNK-1 immunostaining in the control embryos when comparing  
23 control side to DMSO injected side (Supplemental Fig. 1F). These data suggested that

1 AQP-1 expression, and therefore function, promotes efficient neural crest cell invasion  
2 in vivo.

3

#### 4 **Overexpression of Aquaporin-1 in vivo enhances neural crest cell invasion**

5 To further investigate the role of AQP-1 in neural crest migration in vivo, we  
6 overexpressed AQP-1 (via transfection with AQP-1 full length (FL) construct) in  
7 premigratory cranial neural crest cells. Overexpression of AQP-1 caused neural crest  
8 cells to migrate further than control pMES-EGFP transfected neural crest cells at both  
9 12 hours (Fig. 3H, I) and 16 hours (Fig. 3J, K) after transfection. Measurements  
10 confirmed a significant increase in the distance by AQP-1 FL transfected neural crest  
11 cells migrated when compared to pMES transfected neural crest cells analyzed at the  
12 same time points (Fig. 3L, M). To determine whether the increased distance migrated  
13 when AQP-1 was overexpressed was due to an increase in cell speed, we performed in  
14 vivo time-lapse confocal imaging of the migratory streams with five-minute intervals  
15 after control (Gap43-YFP) and AQP-1 FL transfections (Fig. 3N, O; Supplemental Movie  
16 2). Cell tracking confirmed that neural crest cells migrated further and faster within the  
17 invasive front (front 20% of the migratory stream) when transfected with AQP-1 FL as  
18 compared to controls (Fig. 3P, S; Supplemental Movie 2). Interestingly, when neural  
19 crest cells were transfected with AQP-1 FL, they also displayed a decrease in cell  
20 directionality when compared to pMES transfected neural crest cells (Fig. 3Q). To  
21 indicate whether AQP-1 may be playing a role in delamination, the number of  
22 transfected cells was counted at 16 hours. Although there were statistically more AQP-1  
23 transfected neural crest than pMES, the range of cell numbers varied greatly and may

1 be due to differences in transfection efficiency as opposed to a role in delamination (Fig.  
2 3R). Together, these data suggested that AQP-1 is critical to the directed neural crest  
3 cell invasion but they do not reveal the mechanistic basis underlying AQP-1 function  
4 was unclear.

## 6 **Aquaporin-1 stabilizes neural crest cell filopodia**

7 To begin to address the mechanistic basis of AQP-1 function during cranial neural crest  
8 cell migration, we first perturbed AQP-1 function and used spinning disk confocal  
9 microscopy on the lead neural crest cells in vivo to observe any rapid changes in cell  
10 morphology and behavior. Specifically, we collected z-stacks at 20 to 30 second  
11 intervals of neural crest cells transfected with Gap43-mTurquoise2 as well as AQP-1  
12 MO (knockdown), AQP-1 FL (overexpression) or pMES (control) (Fig. 4A, B, J;  
13 Supplemental Movie 3). Images of transfected cells were first processed by creating a  
14 binary mask of single cells in ImageJ using the membrane bound Turquoise2 signal and  
15 then using the CellGeo software (Tsygankov et al., 2014) and additional calculations to  
16 identify and measure filopodia length, position, angle and survival time (Fig. 4C-E).  
17 With knockdown of AQP-1, we find a significant reduction in the number and length of  
18 filopodia in migrating neural crest cells (Fig. 4F, G). In addition, filopodia in cells lacking  
19 AQP-1 retracted at significantly faster rates than control cells leading to less stable  
20 filopodia with a shorter survival time (Fig. 4H, I). In contrast, lead neural crest cells with  
21 an overexpression of AQP-1 resulted in enhanced stable filopodia with reduced  
22 protrusion and retraction rates and a longer survival time (Fig. 4H, I). The average

1 number of filopodia per cell was reduced when AQP-1 was overexpressed but their  
2 length was unchanged (Fig. 4F, G).

3

4 We also examined the direction in which the filopodia extended relative to the direction  
5 of migration of the cell. A vector was created from the base of the filopodia to the tip  
6 and the angle to the direction of motion was calculated (Supplemental Fig. 2C). The  
7 control filopodia were roughly bi-polar in distribution, pointing both towards and away  
8 from the direction of motion as shown on the rose plot though the Rayleigh test does  
9 indicate a uniform distribution ( $p=0.2$ ) (Supplemental Fig. 2A). With overexpression of  
10 AQP-1, the filopodia are found to point randomly in all directions ( $p=0.22$ )  
11 (Supplemental Fig. 2A). Filopodia after knockdown of AQP-1 by MO on average are  
12 directed  $-60^\circ$  degrees rostral from the direction of motion roughly towards BA3  
13 ( $p=4.8 \times 10^{-6}$ ) (Supplemental Fig. 2A). We considered the possibility that the longest  
14 filopodia may be more important for directional migration by comparing the length of the  
15 filopodia found in a  $30^\circ$  window around the direction of motion to the length of filopodia  
16 in all other directions. For control cells, the filopodia in the direction of migration are  
17 significantly longer than the remaining filopodia ( $p=5.9 \times 10^{-9}$ ) (Supplemental Fig. 2B).  
18 However, this association is lost in both overexpression and knockdown of AQP-1 and  
19 the filopodia in the direction of motion are no longer than filopodia elsewhere in the cell  
20 ( $p=0.31$  and  $p=0.2$  respectively) (Supplemental Fig. 2B). These data strongly suggest  
21 that AQP-1 functions to stabilize filopodia in migrating neural crest cells; results in the  
22 literature suggest that this is likely due to water flux (Papadopoulos et al., 2008;  
23 Karlsson et al., 2013; Saadoun et al., 2005).

1

## 2 **Aquaporin-1 influences neural crest cell focal adhesions and ECM degradation**

3 To further explore the role of AQP-1 in neural crest cell invasion, we examined whether  
4 AQP-1 is involved in two important aspects of cell migration: cell–ECM attachment and  
5 ECM degradation. First, we overexpressed AQP-1 in migrating neural crest cells,  
6 isolated those cells from developing embryos and performed RNAseq. The sequencing  
7 results were compared to neural crest cells transfected with pMES only. Significant  
8 pathways affected by AQP-1 expression include many guidance signaling pathways,  
9 such as semaphorins, FGFs, neuregulin and ephrins, as well as the actin cytoskeleton  
10 (Fig. 5A). Members of the AQP family have been shown to promote migration by  
11 facilitating the recycling of integrins and therefore turnover of focal adhesions that are  
12 necessary for cell invasion (Chen et al., 2012). When AQP-1 is overexpressed,  
13 *integrins A8* and *B5* were significantly increased (Supplemental Table 1). Therefore, we  
14 performed IHC for HNK-1, AQP-1 and phosphorylated FAK on cranial neural crest cells  
15 in migrating r4 neural crest in vivo. Confocal imaging with Airyscan detection reveals a  
16 colocalization between the puncta of pFAK and AQP-1 IHC (Pearson’s coefficient 0.74),  
17 indicating a very close physical proximity of these two proteins (Fig. 5C). To further  
18 investigate the possible link of AQP-1 with pFAK and integrins, we performed IHC for  
19 HNK-1, pFAK and integrin B1 after transfection with AQP-1 FL (overexpression) or  
20 pMES (control) in vitro. Using Airyscan confocal microscopy and spot detection  
21 analysis, AQP-1 overexpression leads to less pFAK puncta as well as less integrin B1  
22 puncta on or very near neural crest cell membranes. RNAseq analysis showed that  
23 integrin B1 RNA levels did not change when AQP-1 was overexpressed (Supplemental

1 Table 1). Therefore, this result suggests increased turnover of integrin B1 via  
2 internalization, which would be consistent with previous literature (Chen et al., 2012), or  
3 dissociation of the integrin heterodimers as well as internalization or loss of  
4 phosphorylation of FAK (Fig. 5D).

5  
6 From the RNAseq data, we also focused our attention on ECM related genes as AQP-1,  
7 AQP-3 and AQP-4 have all been shown to be positive regulators of the ECM degrading  
8 molecules, MMPs (Chen et al., 2015; Ding et al., 2011; Jiang et al., 2014; Wei and  
9 Dong, 2015; Xiong et al., 2017; Xu et al., 2011). When AQP-1 is overexpressed in  
10 migrating neural crest cells, *MMP9* as well as members of the ADAMs, including  
11 *ADAM33* are significantly increased (Fig. 5B). To test whether AQP-1 is upstream of  
12 MMP activity, we measured MMP activity from neural crest cells using an in-gel  
13 zymography assay. Specifically, neural tube cultures were exposed to either AZA (AQP-  
14 1 inhibitor), GM6001 (MMP inhibitor) or used as controls. The media from these cultures  
15 was then extracted to determine MMP activity. Neural crest cells exposed to AZA  
16 exhibited a reduction of MMP activity of 73% at a size that most likely matches MMP2  
17 (Fig. 5E; Supplemental Fig. 1G). In comparison, neural crest cells exposed to GM6001  
18 exhibited a reduction of MMP activity of 83%, which was our positive control to show  
19 that the assay was functional (Fig. 5E; Supplemental Fig. 1G). This result was verified  
20 with an in vitro degradation assay, where neural tubes (transfected with AQP-1 FL or  
21 pMES) were plated on top of fluorescently labeled gelatin (Garmon et al., 2018). After  
22 40 hours of incubation, the assays were imaged, and average fluorescent intensity of  
23 the gelatin was quantified as a read out of degradation (Fig. 5F). Neural tubes

1 transfected with pMES significantly degraded gelatin compared to control wells where  
2 no neural tubes were plated as expected (Fig. 5F, G). Transfection with AQP-1 FL  
3 resulted in even higher gelatin degradation, which is consistent with the in gel  
4 zymography (Fig. 5F, G). These data suggest that AQP-1 is involved in the promotion of  
5 integrin turnover and ECM degradation.

6

### 7 **Aquaporin-1 is colocalizes with EphB1 and EphB3 expression in the same** 8 **migrating cranial neural crest cells**

9 Previous work in commissural axon guidance in mouse has shown evidence for the co-  
10 immunoprecipitation of AQP-1 and Eph receptors, namely EphB2, to form a stable  
11 complex within a cell (Cowan et al., 2000). Since Ephs and ephrins are implicated in  
12 axon pathfinding, Cowan and colleagues speculated that aquaporins may function in the  
13 growth cone to help integrate the guidance information elicited by Eph-ephrin clustering  
14 (Cowan et al., 2000). Based on this study, we asked whether the Eph receptors EphB1  
15 and EphB3, previously shown to be highly expressed in the most invasive cranial neural  
16 crest cells (McLennan et al., 2015a), were co-localized with AQP-1 expression in the  
17 same migrating cranial neural crest cells. To address this, we used multiplexed  
18 fluorescence in situ hybridization (RNAscope) to label *AQP-1*, *EphB1*, and *EphB3*  
19 mRNA expression and HNK-1 IHC to quantify co-expression of these three mRNAs in  
20 cranial neural crest cells in vivo (Fig. 6A, B). As before, the HNK-1 channel was used to  
21 segment r4 neural crest from whole mount HH13 embryos (white outlines, Fig. 6A, B)  
22 and spots of *AQP-1*, *EphB1* and *EphB3* mRNA transcripts were counted per cell. When  
23 we quantified the mRNA expression, we found that *AQP-1* mRNA was only found in

1 cells also expressing *EphB1* and/or *EphB3* mRNA though there were many *EphB1*  
2 and/or *EphB3* mRNA positive cells without *AQP-1* mRNA (Fig. 6C). When we quantified  
3 the average number of detected transcripts in migrating neural crest cells, we found that  
4 cells expressing *AQP-1* mRNA had higher number of *EphB1* and *EphB3* mRNA  
5 transcripts than their *AQP-1* negative counterparts (Fig. 6D). By IHC, we can also verify  
6 that *AQP-1* protein and *EphB1/B3* protein co-label the same neural crest cells in vivo  
7 (Fig. 6E-H).

8

### 9 **Aquaporin-1 is involved in the directed migration of neural crest cells**

10 To further explore the hypothesis that *AQP-1* is downstream of guidance, we performed  
11 in vitro cultures where migrating neural crest cells were exposed to BA tissue, a known  
12 source of guidance (Fig. 6I; Supplemental Movie 4). When *AQP-1* was overexpressed  
13 in neural crest cells, they were less directed than untransfected controls in the same  
14 cultures, or in pMES only transfected neural crest cells (Fig. 6I, J; Supplemental Movie  
15 4). This finding is consistent with the loss of directionality observed when *AQP-1* was  
16 overexpressed in neural crest cells in vivo (Fig. 3Q), and the loss of polarized filopodia  
17 in the direction of migration (Supplemental Fig. 2B). One possible explanation for this  
18 result is that by overexpressing *AQP-1* motility is increased due to more *AQP-1*  
19 channels, but these channels are no longer focused by complexing with guidance  
20 receptors. Overall, these data suggest that *AQP-1* is involved in the fast response of  
21 cells to guidance factors, possibly by complexing with guidance receptors, including  
22 *EphB* receptors.



1

2 **Computational modeling predicts that enhanced collective cell invasion is**  
3 **achieved by a combination of increased cell speed, filopodia stabilization and**  
4 **ECM degradation**

5 To test hypothetical mechanistic scenarios by which AQP-1 functions during neural  
6 crest cell invasion, we used a hybrid computational model of cranial neural crest  
7 invasion. The model consists of a discrete, off-lattice model for the cells that is coupled  
8 to a continuum, reaction-diffusion model of the dynamics of a known cranial neural crest  
9 cell chemoattractant (McLennan et al., 2010; VEGF) on a growing domain. The model is  
10 based on our previous studies (McLennan et al., 2015a; McLennan et al., 2012;  
11 McLennan et al., 2015b; McLennan et al., 2017) and is fully described in Supplemental  
12 Data 1. Briefly, we used a two-dimensional approximation of the neural crest cell  
13 migratory domain and incorporated finite size effects by considering cells as hard disks  
14 that are not allowed to overlap (Supplemental Table 2; Supplemental Fig. 3). We used  
15 a fixed time step model (with a time step of 1 minute) during which a cell senses its  
16 environment and moves accordingly. We considered two subpopulations of cells,  
17 namely leaders and followers; leaders undertake a biased random walk up a cell-  
18 induced gradient of chemoattractant (Supplemental Table 2).

19

20 In this study, we modified five parameters, or features, of our model to simulate the  
21 mechanisms by which AQP-1 influences cell migration: cell speed; filopodia stability;  
22 filopodia polarity; filopodia number and ECM degradation (Fig. 7A). Filopodia  
23 stabilization is realized by a leader sampling the microenvironment only every three time

1 steps and moving persistently in between, as opposed to sampling and potentially  
2 moving in a different direction at each time step. Filopodia polarization means that a  
3 leader only stabilizes its filopodium when a cell makes an informed movement towards  
4 a higher concentration of VEGF as opposed to a random movement. Filopodia number  
5 is the number of random directions in which a leader samples the concentration of  
6 chemoattractant per time step. Since our experimental results showed that  
7 overexpression of AQP-1 induced an increase in MMP activity that resulted in ECM  
8 degradation (Fig. 5E-G) we introduced into the model the creation of tunnels in the ECM  
9 (Fig. 7B). This was implemented by recording the histories of leader positions and  
10 defining them as tunnels. Finally, the invasion of cells was assumed to occur on a  
11 uniformly growing rectangular domain whose growth was based on biological  
12 measurements (McLennan et al., 2015a; McLennan et al., 2012).

13  
14 In our computational model we initially quantified changes in the dynamics of cells when  
15 we recapitulated the effects of overexpression and downregulation of AQP-1 by  
16 modulating relevant model parameters. Different combinations of parameter  
17 perturbations are labeled as Model x (x from 1 to 11); the values of parameters for  
18 different models can be found in Figure 7A. In model simulations, we measured the  
19 density of cells along the two-dimensional migratory domain and the likelihood of  
20 migratory stream breakage, defined as the proportion of cells not in chains or tunnels at  
21 the end of a simulation (Fig. 7D). In the control case, the cell speed was set to 62  $\mu\text{m/hr}$ ,  
22 filopodia were not stabilized, and there was a representative number of three filopodia  
23 per cell (Model 1). To simulate AQP-1 overexpression, the cell speed was increased by

1 approximately 30% to 82  $\mu\text{m/hr}$ , filopodia were stabilized and there were two filopodia  
2 per cell (Model 2). To simulate inhibition of AQP-1, the cell speed was decreased to 57  
3  $\mu\text{m/hr}$ , cells had only a single filopodium, which was not stabilized (Model 3). Initially  
4 (Models 1-9), we did not incorporate ECM degradation (i.e. we did not include the  
5 tunneling mechanism. For each model, simulations were run ten times with each  
6 parameter set, and the results at  $t=24$  hours were averaged to account for random  
7 variations. As expected, cells at the front traveled farther when their speed was  
8 increased (Fig. 7C; Model 2). Cells traveled shorter distances when their speed was  
9 reduced to simulate AQP-1 knockdown (Fig. 7C; Model 3). We did, however, observe  
10 an unexpected phenomenon; when the cell speed was increased the simulated cell  
11 migratory streams broke apart more frequently and the model did not sustain collective  
12 cell migration (Fig. 7D). Migratory stream breakage is not observed *in vivo* and therefore  
13 this observation led us to further investigate cell speed versus filopodia dynamics and  
14 the effects upon collective cell migration *in silico*.

15

16 In our simulations, when cell speed was increased, with or without filopodia stabilization,  
17 cells at the front traveled farther compared to the control case (compare Model 4 and  
18 Model 5 with Model 1) but stream breakage was much more likely to occur (Fig. 7D, E).  
19 The number of filopodia (two or three) affected the likelihood of stream breakage at  
20 control cell speeds, with more filopodia resulting in a higher likelihood of breakage but  
21 with little impact upon the distance migrated (compare Model 6 with Model 7) (Fig. 7D,  
22 E). At higher speeds, whether cells had two or three filopodia did not significantly affect  
23 the probability of stream breakage or the distance the cells migrated (compare Model 2

1 with Model 5) (Fig. 7C-E). Stabilization of filopodia increased the farthest distance  
2 traveled by cells regardless of the cell speed. It also noticeably reduced the likelihood of  
3 stream breakage at control cell speeds, with a smaller effect at enhanced speeds  
4 (compare Model 1 with Model 6, and Model 4 with Model 5) (Fig. 7D, E). Additionally,  
5 polarization of filopodia had an insignificant effect on the migration pattern (compare  
6 Model 7 with Model 8 and Model 2 with Model 9) (Fig. 7D, F).

7

8 Since our experimental findings showed that increasing AQP-1 activity led to an increase  
9 in MMP activity, and thus to an increase in degradation of the ECM, we included the  
10 formation of tunnels by leader cells in silico. We found this had no significant effect on  
11 distance the cells migrated, however it did dramatically decrease the percentage of  
12 follower cells not in chains to zero (compare Model 1 with Model 10) (Fig. 7D, G). In  
13 contrast, to simulate overexpression of AQP-1 in the model and include the effects of  
14 increased MMP activity, we increased cell speed, filopodia were stabilized and decreased  
15 in number from three to two, and the leaders generated tunnels for the followers. In this  
16 scenario, our model predicted that the stream is unlikely to break up and invasion is very  
17 robust (compare Model 2 with Model 11) (Fig. 7D, G). Overall, these simulations support  
18 the experimental observations that AQP-1 influences cell migration and invasion in  
19 multiple ways (Fig. 7H; Supplemental Movie 5).

20

21

## 1 **DISCUSSION**

2 Our discovery of high AQP-1 expression within lead cells of the chick cranial neural  
3 crest cell migratory stream (1, 2) led us to examine the function of this water channel  
4 protein. We initially confirmed that *AQP-1* mRNA and protein are both higher in lead  
5 cranial neural crest cells in vivo, and we used state-of-the-art imaging to show that  
6 AQP-1 expression is localized to neural crest cell membranes including cell filopodia.  
7 We tested the hypothesis that AQP-1 regulates cell migration to promote neural crest  
8 cell invasion using gain- and loss-of-function of AQP-1 and quantification of cell  
9 dynamics obtained from time-lapse imaging sessions. We elucidated four important  
10 aspects of AQP-1 function that support its critical in vivo role in neural crest cell  
11 migration.

12  
13 First, we discovered that modulation of AQP-1 expression altered neural crest cell  
14 motility and invasive ability. An increase in AQP-1 expression in premigratory cranial  
15 neural crest cells resulted in higher cell speeds in vitro and enhanced invasion in  
16 vivo (Figs. 2, 3). In contrast, the knockdown of AQP-1 function by MO transfection or  
17 microinjection of the chemical blocker AZA into the neural crest cell migratory  
18 pathway resulted in slower cell speeds in vitro and reduced invasion in vivo (Figs. 2,  
19 3). These results are consistent with previous data that implicated the role of AQP-1  
20 in cell migration and invasion across a wide variety of adult mouse and human  
21 cancer cell types (Saadoun et al., 2005; Chen et al., 2012; Chen et al., 2015; Wei  
22 and Dong, 2015; Xiong et al., 2017; Cao et al., 2006; Hu and Verkman, 2006; Klebe  
23 et al., 2015).

1  
2 Second, we found that AQP-1 promoted neural crest cell invasive ability by  
3 stabilizing filopodia, supporting a function for AQP-1 in enabling cells to bulldoze  
4 through the embryonic microenvironment. Initially, we hypothesized that AQP-1  
5 functions to promote neural crest cell invasion by: (1) rapidly changing the cell  
6 volume and shape to permit the cell to infiltrate between gaps in loosely connected  
7 mesoderm and dense ECM through which cells travel, or; (2) stabilizing cell filopodia  
8 to allow break down and displace the surrounding tissue. In support of (2), we found  
9 a significant reduction in the number and length of neural crest cell filopodia after  
10 AQP-1 knockdown (Fig. 4). Further, neural crest cell filopodia retracted faster and  
11 survived for shorter duration in cells with reduced AQP-1 function (Fig. 4).

12  
13 We did not observe overall cell volume changes in migrating neural crest cells in vivo  
14 by dynamic analysis of three-dimensional cell volumes measured from time-lapse  
15 imaging sessions (data not shown). Given that changes in cell size that are induced  
16 by alterations in external osmolarity have been linked to AQP-1 function in human  
17 vascular smooth muscle cells in culture (Shanahan et al., 1999), we cannot  
18 completely rule cell volume changes out since changes in the dynamic filopodia  
19 volume of migrating neural crest cells may require higher resolution microscopy to  
20 detect. Further, a similar volume of water may flow into or out of control and AQP-1  
21 perturbed neural crest cells as perturbations are not localized to distinct regions of  
22 individual cells.

23

1 Third, we learned that AQP-1 directly influenced neural crest cell adhesion and ECM  
2 degradation, suggesting a mechanistic basis for neural crest cell “bulldozing” through  
3 the microenvironment. In support of this, we showed that AQP-1 and  
4 phosphorylated-FAK were colocalized in migrating neural crest cells, and upon AQP-  
5 1 overexpression, less pFAK and integrin B1 puncta were present on cell surfaces  
6 (Fig. 5). This implicated AQP-1 in the integrin-mediated focal adhesion signaling  
7 pathways previously shown to be important for neural crest cell migration (Desban  
8 and Duband, 1997; Desban et al., 2006; Parsons, 2003). Furthermore, it has been  
9 previously shown that Aquaporin-1 regulates FAK expression in bone marrow  
10 mesenchymal stem cells (Meng et al., 2014). FAK binds directly to integrin B1, and  
11 Aquaporin-2 has been shown to internalize integrin B1 (Chen et al., 2012; Lechertier  
12 and Hodivala-Dilke, 2012). Therefore, in migrating neural crest cells, less integrin B1  
13 and pFAK on cell surfaces when AQP-1 is overexpressed may indicate increased  
14 integrin turnover and less cell adhesion (Fig. 5). AQP-1 perturbation affected the  
15 expression and activity of MMPs in migrating cranial neural crest cells when  
16 measured by RNAseq profiling, in-gel zymography and degradation assay (Fig. 5).  
17 Whether pFAK colocalization with AQP-1 in migrating neural crest cells also plays a  
18 role to initiate downstream intracellular signals, including Eph-ephrins, is unclear  
19 (Carter et al., 2002; Miao et al., 2000) and will be the focus of future studies.  
20 Together, these data clearly demonstrated that AQP-1 promotes neural crest cell  
21 invasion by influencing FAK activity, integrin turnover and ECM degradation.  
22  
23 Fourth, we showed that AQP-1 is involved in directed neural crest cell migration,

1 suggesting that AQP-1 is downstream of a cell's ability to readout guidance factors in  
2 the local microenvironment. AQP-1 and EphB receptors were colocalized in the  
3 same migrating neural crest cells at both the RNA and protein levels (Fig. 6). Neural  
4 crest cell directionality in response to endogenous guidance cues was reduced when  
5 AQP-1 was overexpressed both in vitro and in vivo, as the majority of the AQP-1  
6 water channels were no longer downstream of guidance signals (Figs. 3, 6). Further,  
7 AQP-1 overexpression led to observed neural crest cell filopodia pointing in random  
8 directions (Supplemental Fig. 2). It was not clear whether AQP-1 is enriched in a  
9 directional manner, since although there is higher AQP-1 protein expression in lead  
10 migrating neural crest cells in vivo (Fig. 1H), our super resolution microscopy that  
11 revealed AQP-1 protein expression in neural crest cell filopodia was performed in  
12 vitro in the absence of endogenous guidance cues (Fig. 1E). Future experiments that  
13 dissect the AQP-1 and EphB signaling relationship and explore other guidance  
14 receptors we previously identified by profiling migrating cranial neural crest cells  
15 (McLennan et al., 2015) will help to shed light on this.

16

17 Lastly, our computational model simulations identified cell speed, filopodia stabilization  
18 and ECM degradation as key parameters for controlling neural crest cell invasion in  
19 support of AQP-1 function (Fig. 7). When we increased/decreased cell speed to  
20 simulate AQP-1 gain-of-/loss-of-function, respectively, we observed the intuitive  
21 changes in the maximum distance traveled by cells (Fig. 7; Models 2,3; Supplemental  
22 Movie 5). However, unexpected breakdown of the cell migratory stream occurs in silico  
23 when the cell speed is increased; a pattern that is not observed in vivo (Fig. 3).



1 Examination of cell speed versus filopodial dynamics revealed that stabilization of  
2 filopodia rather than filopodia number or polarity increased the furthest distance traveled  
3 by cells (regardless of speed) and reduced the likelihood of stream separation (Fig. 7).  
4 Thus, our computational model simulations support the role of AQP-1 in promoting  
5 neural crest cell invasion through ECM degradation, stabilization of filopodia and  
6 regulation of cell speed.

7  
8 In summary, our findings implicated four processes of AQP-1 function in neural crest  
9 cell migration: modulated cell speed, stabilized filopodia, cell adhesion and ECM  
10 degradation, and co-localization with cell guidance receptors. Whether these  
11 functions are dependent or independent of AQP-1 functioning as a water channel is  
12 currently unknown, however given the vast recent literature on AQP-1 it is likely to be  
13 related to its water functions. By stabilizing filopodia, increasing MMP-mediated  
14 ECM degradation and controlling adhesions in response to guidance receptors, lead  
15 neural crest cells “bulldoze” through the embryonic microenvironment in a directed  
16 manner. Later emerging neural crest cells are able to follow and collective migration  
17 is maintained. Computational modeling identified cell speed, filopodia stabilization  
18 and ECM degradation as key parameters to promote neural crest cell migration. The  
19 combination of computational modeling with an in vivo dynamic imaging platform  
20 with single cell resolution provides a powerful tool to examine both the upstream  
21 regulation of AQP-1 activity and downstream signaling events in directed cell  
22 migration. With the established high correlation of AQP-1 expression and cancer cell  
23 aggressiveness (Tomita et al., 2017; De Ieso and Yool, 2018), our data of in vivo

- 1 AQP-1 function during embryonic neural crest cell migration and mechanistic basis
- 2 of cell bulldozing offer further details on and illustrate the importance of the function
- 3 of aquaporins in development and cancer.

4

5

6

## 1 **MATERIALS AND METHODS**

### 2 **Embryos**

3 White Leghorn, fertilized chicken eggs (Centurion Poultry, Inc.) were incubated in a  
4 humidified incubator at 38°C to the desired developmental stage (Hamburger and  
5 Hamilton, 1951).

6

### 7 **RNAscope and immunohistochemistry (IHC)**

8 RNAscope on whole chick heads was performed as previously described (Morrison et  
9 al., 2017b). Briefly, HH13 chick embryos were harvested and fixed in 4%  
10 paraformaldehyde for 2 hours. Following a dehydration gradient in methanol, embryos  
11 were stored for 4 days at -20°C before RNAscope protocol began. After rehydration,  
12 embryos were digested in a 0.1x dilution of protease solution in PBS-Tween for 6  
13 minutes at 22°C with gentle agitation. AQP-1, EphB1 and EphB3 RNAscope probes  
14 were designed by Advanced Cell Diagnostics (Newark, CA) against GenBank accession  
15 numbers NM\_001039453.1, NM\_205035.1, XM\_422762.4 respectively. AQP-1 was  
16 labeled with Cy3, EphB1 with Atto488 and EphB3 with Cy5 dyes. As a control, embryos  
17 were processed as described but no probes were used (Supplemental Fig. 1A). After  
18 RNAscope, IHC was performed in a 4% molecular biology grade BSA blocking buffer  
19 using HNK-1 primary antibody (TIB-200 hybridoma cell line, ATCC Cell Lines) in 1:25  
20 concentration overnight incubation at 4°C. Secondary antibody Alexa Fluor 594 Goat  
21 anti-Mouse IgM (A21044, Thermofisher Scientific, Waltham, MA, USA) was used in  
22 1:500 concentration overnight at 4°C. The embryos were then cleared with FRUIT  
23 clearing buffer (Hou et al., 2015) at 60% followed by 80% overnight at 4°C.

1  
2 IHC on cryosections or whole mount chick heads was performed with either Phospho-  
3 FAK (Tyr861) (44-626G, ThermoFisher Scientific) at 1:200 concentration, AQP-1  
4 Millipore AB3272 at 1:50 concentration or EphB1/3 (sc-926, discontinued product,  
5 Santa Cruz Biotechnology, Dallas, TX, USA). Generally, tissue was fixed in 4% PFA  
6 overnight at 4°. After washing in PBS, tissue was blocked with 4% BSA, 0.1% Tween  
7 block for 2 hours at room temperature followed by overnight incubation with primary  
8 antibodies at 4°. After washing in block, secondary antibodies were applied in 1:500  
9 concentration overnight at 4°. After a final wash with PBS, whole heads were mounted  
10 for imaging and cryosections were coverslipped with VECTASHIELD HardSet Antifade  
11 Mounting Medium with DAPI (H-1500, Vector Laboratories, Burlingame, CA). The z  
12 stacks of the collected images were loaded into Imaris 9.20. The images were  
13 segmented using the surface function with HNK-1 setting (settings: grain size at least  
14 0.439 um, largest sphere 1.65 um, threshold automatically detected at upper end, lower  
15 end 110, estimated diameter 6-7um, voxels above 1000). Then, cells were selected at  
16 the back and front (respectively) of the r4 stream. The mean intensity of the HNK-1 was  
17 recorded. The HNK-1 intensity value was normalized from a spot detected outside the  
18 cells on the same slide to account for background. The cells intensity was averaged  
19 together and plotted on a box plot via Origin for the front and the back of the stream.  
20 Secondary antibodies: pFAK – Goat anti rabbit IgG (H+L) (CM405F, Biotium, Fremont,  
21 CA, USA), AQP-1 – F(ab')<sub>2</sub>-Goat anti-Rabbit IgG (H+L) Cross-Adsorbed Secondary  
22 Antibody, Alexa Fluor 546 (A-11071, ThermoFisher Scientific), EphB1/3 – Alexa Fluor  
23 488 Goat anti-Rabbit 488 (A-11008, ThermoFisher Scientific), HNK-1 – Alexa Fluor 647

1 Goat anti-Mouse IgM (A-21238, discontinued product, ThermoFisher Scientific).  
2 Pearson's coefficients for colocalized fluorescence were calculated in Imaris 9.0.0 using  
3 the Coloc module on 3D data sets. Images of pFAK, HNK-1 and AQP-1 IHC from  
4 different regions of the r4 migratory neural crest stream were created using a 40x 1.2NA  
5 objective with Airyscan imaging on a LSM 800 (Zeiss, Jena, Germany). Post Airyscan  
6 processing, a mask was created with the HNK-1 channel to isolate neural crest and  
7 thresholds for pFAK and AQP-1 channels were created to eliminate background. The  
8 Pearson's coefficient for n=5 embryos was recorded and averaged.

9

## 10 **In vitro assays**

11 In vitro neural tube cultures were performed as previously described (McLennan et al.,  
12 2010), using Ham's F-12 Nutrient Mix media (11765054, ThermoFisher Scientific). For  
13 the initial experiments to examine cell speed, DMSO was added to the media for  
14 controls for the AZA (A6011, Sigma-Aldrich, St Louis, MO) experiments because AZA  
15 was solubilized in DMSO. To transfect some cells in the neural tube cultures with AQP-  
16 1 FL, dorsal neural tubes were electroporated in ovo as previously described  
17 (McLennan and Kulesa, 2007) and allowed to recover for 2-4 hours before being  
18 removed and plated in vitro. Alternatively, neural tubes were removed from embryos  
19 and then constructs or morpholinos were electroporated into the tissue using petri dish  
20 platinum electrode for tissues chamber (45-0505, BTX, Holliston, MA, USA), 5 pulses,  
21 60V. Neural tubes were allowed to recover in chamber for 10 minutes and were then  
22 plated. AQP-1 FL construct was designed and built in the lab, using pMES as a  
23 backbone. Prior to neural crest experiments, AQP-1 FL was tested in a chick cell line

1 and shown to overexpress AQP-1 (Supplemental Fig. 1B, C). For the directionality  
2 towards the BA2 tissue experiments, neural tubes were soaked in Hoechst, 1:200  
3 dilution for 5 minutes prior to plating and BA2 tissue was soaked in Dil (V22889,  
4 ThermoFisher Scientific), 1:30 dilution for 30 minutes. Time-lapses of cultures were  
5 taken on a LSM 710, LSM 780 or LSM 800 (Zeiss), 2.5 minute intervals, single z-  
6 planes. For IHC on in vitro cultures, the same antibodies and protocols were followed as  
7 for cryosections and whole mount embryos, however the incubation times were shorter.  
8 In vitro cultures were fixed with 4% paraformaldehyde for 20 minutes. Cultures were  
9 incubated with primary and secondary antibodies for 1 hour each. Images were taken  
10 using confocal microscopy and Airyscan detection with a 40x 1.2NA water immersion  
11 objective. Due to the lengthy timing of collecting Airyscan z stacks and to reduce  
12 possible photobleaching, this imaging was not performed for the entire cell but focused  
13 on the cell membranes against the fibronectin-coated dish surface.  
14 The z stacks of the collected images were loaded into Imaris 9.20. The cells were  
15 segmented using the surface function to manually outline the shape of the cell. Then,  
16 spots were detected on each the integrin and pFAK channels. The integrin channel  
17 spots included a diameter of .6um spot with background subtraction and a quality filter  
18 was picked using a statistical upper and lower threshold break in the data. The pFAK  
19 spots were detected using .4um spots and background subtraction with the quality filter  
20 was picked using a statistical upper and lower threshold break in the data. The number  
21 of spots for each cell was recorded for pFAK and integrin channels then an average  
22 was calculated for each data set. The data was then plotted on a box plot via Origin.  
23 For the neural tube cultures with DMSO, AZA or AQP-1 FL, cells were manually tracked

1 using “Spot” detection in Imaris for  $\geq 6$  hours. The spots were set to  $\geq 9$   $\mu\text{m}$  in size. The  
2 mean speed and displacement of each track was calculated using Imaris (Bitplane).  
3 Straightness equals displacement of track divided by length of track. The box plots in  
4 each figure were generated by using the values from each dataset indicated. X  
5 indicates outliers, and the box plots and whiskers indicate the quartiles and range,  
6 respectively, of each dataset. P-values were calculated using a standard Student’s *t* test  
7 or paired *t* test. Data distribution was assumed to be normal, but this was not formally  
8 tested.

9

## 10 **In ovo injections, electroporations and analysis**

11 AZA (500  $\mu\text{M}$ ) was injected into multiple sites of the mesoderm on one side adjacent to  
12 the hindbrain region of HH8-9 embryos. For control injections, the same injections were  
13 performed using DMSO. After 24 hours reincubation, embryos were fixed in 4%  
14 paraformaldehyde for 2 hours at room temperature and then immunohistochemistry was  
15 performed for HNK-1 as described above. Each cranial region of injected embryos was  
16 then cut down the midline and each half mounted in a glass slide as previously  
17 described (Teddy and Kulesa, 2004). Both halves of the cranial region of each embryo  
18 were imaged on a LSM 800 (Zeiss) so that injected and control halves of each embryo  
19 could be compared. In ovo electroporations were performed as previously described  
20 (McLennan and Kulesa, 2007). Fluorescein-tagged AQP-1 and control morpholinos  
21 were designed by, and obtained from, Gene Tools, LLC (Philomath, OR, USA). H2B  
22 mCherry (2.5 $\mu\text{g}/\mu\text{l}$ ) and morpholinos (0.5 $\text{mM}$ ) were injected and electroporated at HH8-  
23 9 and reincubated for 20 hours before being fixed, processed for HNK-1 and imaged as

1 described above. An empty EGFP vector, pMES, was used as control to AQP-1 FL, as  
2 AQP-1 FL was inserted into the pMES vector. pMES and AQP-1 FL were either  
3 injected and electroporated with Dil before being reincubated for 12 hours or injected  
4 and electroporated without Dil before being reincubated for 16 hours. Time-lapses were  
5 performed as previously described (McKinney et al., 2013). We calculated the  
6 percentage of area covered using the “Surfaces” function of Imaris (Bitplane) to create a  
7 surface mask by manually drawing the outline of the whole branchial arch. Next, we  
8 calculated the area of the HNK-1 fluorescence signal using the masked arch surface.  
9 We set a consistent intensity threshold to the same value for each dataset, a surface  
10 grain size of 1  $\mu\text{m}$  was set, the diameter of the largest sphere was set to 1  $\mu\text{m}$ , and then  
11 the automatic “Surfaces” function was applied. We calculated the percentage of the  
12 front of arch the HNK-1 signal covered by comparing the two values in the front 50% of  
13 the stream. For electroporated embryos, cells were automatically detected using the  
14 “Spot” function in Imaris. The spots were set to  $\geq 9 \mu\text{m}$  in size. The spots were counted  
15 in the front 50% of the stream. The percentage of total spots versus cells in the whole  
16 stream was calculated. The percentage of distance the cells migrated was calculated  
17 by measuring the total distance of the migratory route and measuring what distance the  
18 transfected cells migrated. This was calculated on 3D z-stacks using the measurement  
19 tool in Imaris. The box plots in each figure were generated by using the values from  
20 each dataset indicated. X indicates outliers, and the box plots and whiskers indicate the  
21 quartiles and range, respectively, of each dataset. P-values were calculated using a  
22 standard Student’s *t* test or paired *t* test. Data distribution was assumed to be normal,  
23 but this was not formally tested.



1  
2  
3  
4  
5  
6  
7  
8  
9  
10  
11  
12  
13  
14  
15  
16  
17  
18  
19  
20  
21  
22  
23

## **Spinning Disk Imaging and Analysis**

HH13 chick embryos were mounted dorsal side down on glass bottomed dishes with a grease-sealed Teflon membrane over the top to preserve humidity (Rupp and Kulesa, 2007). Samples were placed inside a heated chamber around a spinning disk confocal microscope (PerkinElmer, Ultraview), allowed to acclimate to the chamber, and 2 channel imaging proceeded until any sign of phototoxicity was observed. Cells in the front 10% of the migratory r4 neural crest stream were chosen for imaging. Images were collected with a 40x 1.2NA water immersion objective in 1 um Z-steps for up to 15 um total depth in either 20 or 30 second increments. Time-lapse data were analyzed in a combination of Imaris (Bitplane AG) and ImageJ. If cells were overlapped in Z, Imaris 3D imaging was used to create a mask of the cell of interest which was then projected onto 2D. A projected image of the cell was imported into ImageJ and after smoothing and background subtraction, an 8-bit binary mask was created using the Gap-mTurquoise2 fluorescence. Minor adjustments to the mask were made by hand for extremely thin filopodia or touching cells. The time-lapse masked image was imported into a modified version of the CellGeo software (Tsygankov et al., 2014) that did not use the java enabled GUI but allowed for parameter adjustment using the same algorithms. BisectoGraph and FiloTrak modules were used and parameters of 20 smooth, 1 CrR, 1 CutOff, 9 Critical length, 5.5 critical width were used. Filopodia were tracked manually. The remainder of analysis was written in MATLAB (Mathworks Inc) to collect filopodia data from multiple cells under each condition.

## 1 **Cytometry, RNA-seq and Analysis**

2 Premigratory neural crest were electroporated with either AQP-1 FL or pMES and eggs  
3 re-incubated for 24 hours. The neural crest stream adjacent in rhombomere 4 was  
4 isolated from healthy ~HH15 embryos. Five pMES transfected embryos were pooled for  
5 each of the 3 biological replicates (n=15 total). Four AQP-1 FL embryos were pooled for  
6 each of the 3 biological replicates (n=12 total). Tissue was dissociated as previously  
7 described (McLennan et al., 2015a). Cells were isolated by FACS, which included  
8 forward scatter, side scatter, pulse width, live/dead stain (7AAD) and YFP gates as  
9 previously described (McLennan et al., 2015a; Morrison et al., 2017a). Cells were  
10 sorted directly into 7ul of Clontech lysis solution containing 0.05% RNase inhibitor.  
11 Following lysis for 5 minutes at room temperature, lysates were immediately frozen on  
12 dry ice and stored at -80C. Bulk RNA-seq lysates were thawed on ice. cDNA synthesis  
13 and library preparation were performed with SMART-seq v4 Ultra Low Input RNA-seq  
14 (634891, Takara, Kusatsu, Shiga, Japan) and Nextera XT DNA sample prep and  
15 indexing library preparation kits as recommended by the manufacturer (FC-131-2001,  
16 FC-131-2004, and FC-131-1096, Illumina, San Diego, CA). Resulting short fragment  
17 libraries were checked for quality and quantity using a Bioanalyzer (Agilent) and Qubit  
18 Fluorometer (Life Technologies). Libraries were pooled, re-quantified and sequenced as  
19 50bp single reads on 2 lanes of the Illumina HiSeq 2500 in High Output mode using  
20 HiSeq Control Software v2.2.58 (illumine). Following sequencing, Illumina Primary  
21 Analysis version RTA v1.18.64 and bcl2fastq2 v2.18 were run to demultiplex reads for  
22 all libraries and generate FASTQ files. More than 3 million total alignments were  
23 produced per sample. Single end 51-base reads were aligned to the chicken genome

1 galGal4 from UCSC with annotations from Ensembl 84 using STAR (2.5.2b) with  
2 options `-alignEndsType EndToEnd` and `sjdbScore 2`. Downstream analysis was done in  
3 R (3.4.1). Differential expression analysis was performed using the edgeR package  
4 (3.18.1). Genes were denoted as differentially expressed if they had a p-value less than  
5 .05 and a fold change greater than 1.5-fold (absolute value). Gene ontology enrichment  
6 was done using a hypergeometric test on lists of differentially expressed genes. The  
7 data discussed in this publication have been deposited in NCBI's Gene Expression  
8 Omnibus and are accessible through GEO Series accession number GSE121131  
9 (<https://www.ncbi.nlm.nih.gov/geo/query/acc.cgi?acc=GSE121131>).

10

### 11 **In gel zymography**

12 To achieve high levels of MMP secretion from neural crest cells grown in culture, neural  
13 tubes were isolated, plated onto the bottom of 4 well dishes (176740, ThermoFisher  
14 Scientific) with no coating, covered in 250 ul of Ham's F-12 media. N=39 neural tubes  
15 exposed to 100 uM AZA, n=39 neural tubes exposed to DMSO, 0.05 ul in 1 mL, as  
16 control for AZA, n=32 neural tubes exposed to 50 umol/L GM6001 (Anderson et al.,  
17 2006), n=32 neural tubes exposed to DMSO, 1 ul in 1 mL, as control for GM6001. After  
18 24 hours of incubation, the media was harvested. Protein in media was concentrated  
19 using 3K Pierce concentrator (88512, ThermoFisher Scientific), and then used in gel  
20 zymography following suppliers protocol (ZY00100BOX, LC2670, LC2671, LC2675,  
21 LC2676, ThermoFisher Scientific). The substrate was gelatin. Importantly, an image of  
22 the gel prior to colloidal blue staining (LC6025, ThermoFisher Scientific) was taken so  
23 that the protein ladder could be clearly seen for determining protein size after staining.

1 Quantification of the bands on the gel image were performed using ImageJ and a  
2 protocol from Protocol Place (<http://protocol-place.com/assays/gelatin-zymography/>).

3

#### 4 **Degradation assay**

5 Degradation assay was performed using QCM Gelatin Invadopodia Assay (ECM671,  
6 Millipore, Burlington, MA, USA). Following the manufacturers protocol, Cy3-labeled  
7 gelatin coated wells in 8-well chambered slides (80821, Ibidi, Martinsried, Germany).  
8 The protocol was slightly modified by heating all the gelatin to 60 degrees Celsius so  
9 that there was no issue in room temperature and warm gelatin not mixing fully. To  
10 optimize cell adhesion, fibronectin was then added over the gelatin as previously  
11 described (Garmon et al., 2018). 15 neural tubes (transfected with either pMES or  
12 AQP-1 FL) were plated into each well with 500ul of media and incubated for 40 hours.  
13 For controls, some wells received no neural tubes, but were still incubated for 40 hours  
14 with 500ul of media. Cultures were fixed with 4% paraformaldehyde for 20 minutes and  
15 then imaged. MMP2 and MMP9 are secreted proteases and possible gelatin  
16 degradation will occur throughout each well, not just where neural crest cells are  
17 migrating. Therefore, Cy3-labeled gelatin was imaged at 5 randomly chosen areas of  
18 each well using a 40x 1.2NA objective, n=3 wells per condition. The z-stack images  
19 were loaded into Imaris 9.20. A surface rendering was created on the whole Cy3  
20 gelatin channel throughout the whole image with the automatic settings used to detect  
21 the surface using voxel totals above 10. The average intensity across the whole image  
22 for the Cy3 channel was recorded. An average was taken from each condition and a  
23 box plot was made in Origin.

1 **ACKNOWLEDGEMENTS**

2 PMK would like to acknowledge kind and generous funding from the Stowers Institute  
3 for Medical Research. We also thank members of the Microscopy, Histology and  
4 Molecular Biology core facilities and our Scientific Illustrator, Mark Miller, at the Stowers  
5 Institute for Medical Research.

6

7 **AUTHOR CONTRIBUTIONS**

8 R McLennan performed in vitro and in vivo functional perturbations of AQP-1, isolation  
9 of electroporated cells for FACS and RNA-seq, in vivo AQP-1 and Eph IHC, in vitro  
10 pFAK and integrin B1 IHC after AQP-1 FL or pMES transfection, degradation assays  
11 and corresponding imaging. MC McKinney performed RNAscope experiments,  
12 filopodia dynamics, pFAK IHC on wildtype neural crest cells and analysis on these  
13 experiments. DA Ridenour and CA Manthe built and tested the AQP-1 full length  
14 construct. JM Teddy performed the image analysis and measurements. JA Morrison  
15 and R McLennan performed cell dissociation and analysis of RNA-seq data. JC  
16 Kasemeier and R McLennan performed the in gel zymography experiments. JM Teddy,  
17 DA Ridenour and CA Manthe performed the initial time-lapses. R Giniunaite performed  
18 the modeling simulations under the supervision and guidance of M Robinson, RE Baker  
19 and PK Maini. All authors discussed and interpreted the results. R McLennan and PM  
20 Kulesa wrote the manuscript and generated the figures with critical comments and  
21 suggestions from JA Morrison, JM Teddy and MC McKinney. PM Kulesa supervised  
22 the overall project. All authors read and approved the final manuscript.

23

1 **COMPETING INTERESTS**

2 The authors declare no competing interests.

3

## 1 REFERENCES

- 2
- 3 Agre, P, Sasaki, S, Chrispeels, MJ. Aquaporins: a family of water channel proteins. *Am*
- 4 *J Physiol.* 1993 265(3 Pt 2):F461.
- 5 Ameli, PA, Madan, M, Chigurupati, S, Yu, A, Chan, SL, Pattisapu, JV. Effect of
- 6 acetazolamide on aquaporin-1 and fluid flow in cultured choroid plexus. *Acta Neurochir*
- 7 *Suppl.* 2012 113:59-64.
- 8 Anderson, RB, Turner, KN, Nikonenko, AG, Hemperly, J, Schachner, M, Young, HM.
- 9 The cell adhesion molecule I1 is required for chain migration of neural crest cells in the
- 10 developing mouse gut. *Gastroenterology.* 2006 130(4):1221-32.
- 11 Bin, K, Shi-Peng, Z. Acetazolamide inhibits aquaporin-1 expression and colon cancer
- 12 xenograft tumor growth. *Hepatogastroenterology.* 2011 58(110-111):1502-6.
- 13 Cai, L, Chen, WN, Li, R, Hu, CM, Lei, C, Li, CM. Therapeutic effect of acetazolamide,
- 14 an aquaporin 1 inhibitor, on adjuvant-induced arthritis in rats by inhibiting NF- $\kappa$ B signal
- 15 pathway. *Immunopharmacol Immunotoxicol.* 2018 40(2):117-125.
- 16 Cao, C, Sun, Y, Healey, S, Bi, Z, Hu, G, Wan, S, Kouttab, N, Chu, W, Wan, Y. EGFR-
- 17 mediated expression of aquaporin-3 is involved in human skin fibroblast migration.
- 18 *Biochem J.* 2006 400(2):225-34.
- 19 Carter, N, Nakamoto, T, Hirai, H, Hunter, T. EphrinA1-induced cytoskeletal re-
- 20 organization requires FAK and p130(cas). *Nat Cell Biol.* 2002 4(8):565-73.
- 21 Chen, Y, Rice, W, Gu, Z, Li, J, Huang, J, Brenner, MB, Van Hoek, A, Xiong, J,
- 22 Gundersen, GG, Norman, JC, Hsu, VW, Fenton, RA, Brown, D, Lu, HA. Aquaporin 2
- 23 promotes cell migration and epithelial morphogenesis. *J Am Soc Nephrol.*
- 24 2012 23(9):1506-17.
- 25 Chen, J, Wang, Z, Xu, D, Liu, Y, Gao, Y. Aquaporin 3 promotes prostate cancer cell
- 26 motility and invasion via extracellular signal-regulated kinase 1/2-mediated matrix
- 27 metalloproteinase-3 secretion. *Mol Med Rep.* 2015 11(4):2882-8.
- 28 Condeelis, J. Life at the leading edge: the formation of cell protrusions. *Annu Rev Cell*
- 29 *Biol.* 1993 9:411-44.
- 30 Cowan, CA, Yokoyama, N, Bianchi, LM, Henkemeyer, M, Fritzsche, B. EphB2 guides
- 31 axons at the midline and is necessary for normal vestibular function. *Neuron.* 2000
- 32 26(2):417-30.
- 33 De Ieso, ML, Yool, AJ. Mechanisms of Aquaporin-Facilitated Cancer Invasion and
- 34 Metastasis. *Front Chem.* 2018 6:135.
- 35 Desban, N, and Duband, JL. Avian neural crest cell migration on laminin: interaction of
- 36 the alpha1beta1 integrin with distinct laminin-1 domains mediates different adhesive
- 37 responses. *J Cell Sci.* 1997 110( Pt 21):2729-44.
- 38 Desban, N, Lissitzky, JC, Rousselle, P, Duband, JL. alpha1beta1-integrin engagement
- 39 to distinct laminin-1 domains orchestrates spreading, migration and survival of neural
- 40 crest cells through independent signaling pathways. *J Cell Sci.* 2006 119(Pt 15):3206-
- 41 18.
- 42 Ding, T, Ma, Y, Li, W, Liu, X, Ying, G, Fu, L, Gu, F. Role of aquaporin-4 in the regulation
- 43 of migration and invasion of human glioma cells. *Int J Oncol.* 2011 38(6):1521-31.
- 44 Garmon, T, Wittling, M, Nie, S. MMP14 Regulates Cranial Neural Crest Epithelial-to-
- 45 Mesenchymal Transition and Migration. *Dev Dyn.* 2018 247(9):1083-1092.

- 1 Gustafsson MGL, Shao L, Carlton PM, Wang, CLR, Golubovskaya, IN, Cande, WZ,  
2 Agard, DA, Sedat, JW. Three-Dimensional Resolution Doubling in Wide-Field  
3 Fluorescence Microscopy by Structured Illumination. *Biophys. J.* 2008 *94*:4957-4970.  
4 Hamburger, V, Hamilton, HL. A series of normal stages in the development of the chick  
5 embryo. *J Morphol.* 1951 *88*(1):49-92.  
6 Hou, B, Zhang, D, Zhao, S, Wei, M, Yang, Z, Wang, S, Wang, J, Zhang, X, Liu, B, Fan,  
7 L, Li, Y, Qiu, Z, Zhang, C, Jiang, T. Scalable and Dil-compatible optical clearance of the  
8 mammalian brain. *Front Neuroanat.* 2015 *9*:19.  
9 Hu, J, Verkman, AS. Increased migration and metastatic potential of tumor cells  
10 expressing aquaporin water channels. *FASEB J.* 2006 *20*(11):1892-4.  
11 Huber, VJ, Tsujita, M, Yamazaki, M, Sakimura, K, Nakada, T. Identification of  
12 arylsulfonamides as Aquaporin 4 inhibitors. *Bioorg Med Chem Lett.* 2007 *17*(5):1270-3.  
13 Ishibashi, K, Kondo, S, Hara, S, Morishita, Y. The evolutionary aspects of aquaporin  
14 family. *Am J Physiol Regul Integr Comp Physiol.* 2011 *300*(3):R566-76.  
15 Jiang, B, Li, Z, Zhang, W, Wang, H, Zhi, X, Feng, J, Chen, Z, Zhu, Y, Yang, L, Xu, H,  
16 Xu, Z. miR-874 Inhibits cell proliferation, migration and invasion through  
17 targeting aquaporin-3 in gastric cancer. *J Gastroenterol.* 2014 *49*(6):1011-25.  
18 Karlsson, T, Bolshakova, A, Magalhães, MA, Loitto, VM, Magnusson, KE. Fluxes of  
19 water through aquaporin 9 weaken membrane-cytoskeleton anchorage and promote  
20 formation of membrane protrusions. *PLoS One.* 2013 *8*(4):e59901.  
21 Klebe, S, Griggs, K, Cheng, Y, Drimi, J, Henderson, DW, Reid, G. Blockade of  
22 aquaporin 1 inhibits proliferation, motility, and metastatic potential of mesothelioma in  
23 vitro but not in an in vivo model. *Dis Markers.* 2015 *2015*:286719.  
24 Lechertier, T, Hodivala-Dilke, K. Focal adhesion kinase and tumour angiogenesis. *J*  
25 *Pathol.* 2012 *226*(2):404-12.  
26 McKinney, MC, Fukatsu, K, Morrison, J, McLennan, R, Bronner, ME, Kulesa, PM.  
27 Evidence for dynamic rearrangements but lack of fate or position restrictions in  
28 premigratory avian trunk neural crest. *Development.* 2013 *140*(4):820-30.  
29 McLennan, R, Bailey, CM, Schumacher, LJ, Teddy, JM, Morrison, JA, Kasemeier-  
30 Kulesa, JC, Wolfe, LA, Gogol, MM, Baker, RE, Maini, PK, Kulesa, PM. DAN (NBL1)  
31 promotes collective neural crest migration by restraining uncontrolled invasion. *J Cell*  
32 *Biol.* 2017 *216*(10):3339-3354.  
33 McLennan, R, Dyson, L, Prather, KW, Morrison, JA, Baker, RE, Maini, PK, Kulesa, PM.  
34 Multiscale mechanisms of cell migration during development: theory and experiment.  
35 *Development.* 2012 *139*(16):2935-44.  
36 McLennan, R, Kulesa, PM. In vivo analysis reveals a critical role for neuropilin-1 in  
37 cranial neural crest cell migration in chick. *Dev Biol.* 2007 *301*(1):227-39.  
38 McLennan, R, Schumacher, LJ, Morrison, JA, Teddy, JM, Ridenour, DA, Box, AC,  
39 Semerad, CL, Li, H, McDowell, W, Kay, D, Maini, PK, Baker, RE, Kulesa, PM. Neural  
40 crest migration is driven by a few trailblazer cells with a unique molecular signature  
41 narrowly confined to the invasive front. *Development.* 2015a *142*(11):2014-25.  
42 McLennan, R, Schumacher, LJ, Morrison, JA, Teddy, JM, Ridenour, DA, Box, AC,  
43 Semerad, CL, Li, H, McDowell, W, Kay, D, Maini, PK, Baker, RE, Kulesa, PM. VEGF  
44 signals induce trailblazer cell identity that drives neural crest migration. *Dev Biol.* 2015b  
45 *407*(1):12-25.



- 1 McLennan, R, Teddy, JM, Kasemeier-Kulesa, JC, Romine, MH, Kulesa, PM. Vascular  
2 endothelial growth factor (VEGF) regulates cranial neural crest migration in vivo. *Dev*  
3 *Biol.* 2010 339(1):114-25.
- 4 Meng, F, Rui, Y, Xu, L, Wan, C, Jiang, X, Li, G. Aqp1 enhances migration of bone  
5 marrow mesenchymal stem cells through regulation of FAK and  $\beta$ -catenin. *Stem Cells*  
6 *Dev.* 2014 23(1):66-75.
- 7 Miao, H, Burnett, E, Kinch, M, Simon, E, Wang, B. Activation of EphA2 kinase  
8 suppresses integrin function and causes focal-adhesion-kinase dephosphorylation. *Nat*  
9 *Cell Biol.* 2000 2(2):62-9.
- 10 Morrison, JA, McKinney, MC, Kulesa, PM. Resolving in vivo gene expression during  
11 collective cell migration using an integrated RNAscope, immunohistochemistry and  
12 tissue clearing method. *Mech Dev.* 2017b 148:100-106.
- 13 Morrison, JA, McLennan, R, Wolfe, LA, Gogol, MM, Meier, S, McKinney, MC, Teddy,  
14 JM, Holmes, L, Semerad, CL, Box, AC, Li, H, Hall, KE, Perera, AG, Kulesa, PM. Single-  
15 cell transcriptome analysis of avian neural crest migration reveals signatures of invasion  
16 and molecular transitions. *Elife.* 2017a 6. pii: e28415.
- 17 Papadopoulos, MC, Saadoun, S, Verkman, AS. Aquaporins and cell migration. *Pflugers*  
18 *Arch.* 2008 456(4):693-700.
- 19 Parsons, JT. Focal adhesion kinase: the first ten years. *J Cell Sci.* 2003 116(Pt 8):1409-  
20 16.
- 21 Rupp, PA, Kulesa, PM. High-Resolution, Intravital 4D Confocal Time-Lapse Imaging in  
22 Avian Embryos Using a Teflon Culture Chamber Design. *CSH Protoc.* 2007  
23 2007:pdb.prot4790.
- 24 Saadoun, S, Papadopoulos, MC, Hara-Chikuma, M, Verkman, AS. Impairment of  
25 angiogenesis and cell migration by targeted aquaporin-1 gene disruption. *Nature.* 2005  
26 434(7034):786-92.
- 27 Shanahan, CM, Connolly, DL, Tyson, KL, Cary, NR, Osbourn, JK, Agre, P, Weissberg,  
28 PL. Aquaporin-1 is expressed by vascular smooth muscle cells and mediates rapid  
29 water transport across vascular cell membranes. *J Vasc Res.* 1999 36(5):353-62.
- 30 Stroka, KM, Jiang, H, Chen, SH, Tong, Z, Wirtz, D, Sun, SX, Konstantopoulos, K. Water  
31 permeation drives tumor cell migration in confined microenvironments. *Cell.*  
32 2014 157(3):611-23.
- 33 Teddy, JM, Kulesa, PM. In vivo evidence for short- and long-range cell communication  
34 in cranial neural crest cells. *Development.* 2004 131(24):6141-51.
- 35 Tomita, Y, Dorward, H, Yool, AJ, Smith, E, Townsend, AR, Price, TJ, Hardingham, JE.  
36 Role of Aquaporin 1 signaling in cancer development and progression. *Int J Mol Sci*  
37 2017 18(2). Pii:E299.
- 38 Tsygankov, D, Bilancia, CG, Vitriol, EA, Hahn, KM, Peifer, M, Elston, TC. CellGeo: a  
39 computational platform for the analysis of shape changes in cells with complex  
40 geometries. *J Cell Biol.* 2014 204(3):443-60.
- 41 Verkman, AS. Aquaporins: translating bench research to human disease. *J Exp Biol.*  
42 2009 212:1707-15.
- 43 Wei, X, Dong, J. Aquaporin 1 promotes the proliferation and migration of lung cancer  
44 cell in vitro. *Oncol Rep.* 2015 34(3):1440-8.
- 45 Woessner, JF Jr. Quantification of matrix metalloproteinases in tissue samples.  
46 *Methods Enzymol.* 1995 248:510-28.

- 1 Xiong, G, Chen, X, Zhang, Q, Fang, Y, Chen, W, Li, C, Zhang, J. RNA interference  
2 influenced the proliferation and invasion of XWLC-05 lung cancer cells through  
3 inhibiting aquaporin 3. *Biochem Biophys Res Commun.* 2017 *485*(3):627-634.  
4 Xu, H, Xu, Y, Zhang, W, Shen, L, Yang, L, Xu, Z. Aquaporin-3 positively regulates  
5 matrix metalloproteinases via PI3K/AKT signal pathway in human gastric carcinoma  
6 SGC7901 cells. *J Exp Clin Cancer Res.* 2011 *30*:86.  
7 Zhang, J, An, Y, Gao, J, Han, J, Pan, X, Pan, Y, Tie, L, Li, X. Aquaporin-1 translocation  
8 and degradation mediates the water transportation mechanism of acetazolamide. *PLoS*  
9 *One.* 2012 *7*(9):e45976.

10

11

12

## 1 **FIGURE LEGENDS**

2 **Figure 1: Aquaporin-1 is expressed by neural crest cells at the invasive front of**  
3 **the migratory stream and it located in filopodia.** (A-C) Expression of *AQP-1* mRNA  
4 by RNAscope (B) in migrating cranial neural crest cells co-labeled with HNK-1 (A) with  
5 number of *AQP-1* transcripts per neural crest cell counted (C). Bar=30  $\mu$ m. (D)  
6 Quantification of the number of *AQP-1* mRNA transcripts per cell versus distance from  
7 the neural tube. n $\sim$ 7500 cells, n=10 embryos. (E) High resolution image of the neural  
8 crest cell protrusions in vitro showing AQP-1 protein (green) in the filopodia  
9 (arrowheads). Bar=5  $\mu$ m and 2  $\mu$ m for inset. (F) Schematic representation of transverse  
10 section and high resolution image of a migrating neural crest cell (red) at HH11 with  
11 AQP-1 protein (green). Bar=10  $\mu$ m. (G) Schematic representation of transverse section  
12 and migrating neural crest cells (red) at HH15 with AQP-1 protein (green). AQP-1 rich  
13 neural crest marked with arrowhead and asterisk. Bar=20  $\mu$ m. (H) Quantification of the  
14 AQP-1 protein intensity versus HNK-1 intensity from transverse cryostat sections, n=70  
15 leader cells, n=51 follower cells.

16

17 **Figure 2: AQP-1 modifies neural crest cell speed in vitro.** (A) Schematic  
18 representation of experimental setup. (B) Representative images of in vitro neural crest  
19 cell time-lapses with neural crest cells exposed to DMSO (control for AZA treatment),  
20 AZA and transfected with AQP-1 FL. Bar=50  $\mu$ m. (C) Box plot of the Speed (microns/hr)  
21 of neural crest cells with overexpression of AQP-1 (red, n=70 cells) and corresponding  
22 controls (black, n=44 cells), AQP-1 inhibition (pink, n=57 cells) and corresponding  
23 controls (blue, n=43 cells). (D) Box plot of the Straightness of neural crest cells with

1 overexpression of AQP-1 (red, n=71 cells) and corresponding controls (black, n=31  
2 cells), AQP-1 inhibition (pink, n=26 cells) and corresponding controls (blue, n=27 cells).  
3 (E) Representative tracks of neural crest cells with AQP-1 inhibition (pink) and  
4 corresponding DMSO controls (blue). Start points are marked with circles, end points  
5 are marked with squares. (F) Representative tracks of neural crest cells with  
6 overexpression of AQP-1 (red) and corresponding controls (black). Start points are  
7 marked with circles, end points are marked with squares. nt, neural tube; AZA,  
8 Acetazolamide; ctrl, control; t, time; hrs, hours.

9

10 **Figure 3: Neural crest cell migration is decreased when AQP-1 is knocked down**  
11 **and increased when AQP-1 is overexpressed in vivo.** (A) Box plot of the distance  
12 migrated by neural crest cells as a percentage of the whole stream, n=6 embryos per  
13 treatment. (B) Box plot of the percent area of the branchial arch (front 50% of the  
14 stream) containing HNK-1 positive neural crest cells, n=6 embryos per treatment. (C)  
15 HH14 embryo in which neural crest cells (red) are transfected with control MO (green).  
16 Bar=50 um. (D) HH14 embryo in which neural crest cells (red) are transfected with  
17 AQP-1 MO (green). Bar=50 um. (E) Box plot of the percentage of neural crest cells that  
18 migrate into the branchial arches, n=15 embryos per treatment. (F) HNK-1 label of  
19 HH15 embryo after injection of AZA into the paraxial mesoderm, control and injected  
20 sides shown. Bar=50 um. (G) HNK-1 label of HH15 embryo after control injection of  
21 DMSO into the paraxial mesoderm, control and injected sides shown. Bar=50 um. (H)  
22 Neural crest migration 12 hours after premigratory neural crest cells were labeled with  
23 Dil (red) and transfected with pMES (green). \*, end of stream. Bar=50 um. (I) Neural

1 crest migration 12 hours after premigratory neural crest cells were labeled with Dil (red)  
2 and transfected with AQP-1 FL (green). \*, end of stream. Bar=50 um. (J) Neural crest  
3 migration 16 hours after premigratory neural transfected with pMES (green) and then  
4 labeled with HNK-1 (red). Bar=50 um. (K) Neural crest migration 16 hours after  
5 premigratory neural transfected with AQP-1 FL (green) and then labeled with HNK-1  
6 (red). Bar=50 um. (L) Box plot of the distance migrated by control (pMES) and AQP-1  
7 FL transfected neural crest cells 12 hours after transfection, n=16 pMES embryos, n=15  
8 AQP-1 FL embryos. (M) Box plot of the distance migrated by control (pMES) and AQP-1  
9 FL transfected neural crest cells 16 hours after transfection, n=11 pMES embryos, n=15  
10 AQP-1 FL embryos. (N) Selected images from a time-lapse showing neural crest cells  
11 migrating into paraxial mesoderm transfected with a nuclear marker (H2B mCherry, red)  
12 and Gap43-YFP (green). \*, most invasive cell. Bar=20 um. (O) Selected images from a  
13 time-lapse showing neural crest cells migrating into paraxial mesoderm transfected with  
14 a nuclear marker (H2B mCherry, red) and AQP-1 FL (green). \*, most invasive cell.  
15 Bar=20 um. (P) Box plot of the speed of neural crest cells migrating at the front of the  
16 stream into paraxial mesoderm, n=16 cells for control, n=11 cells overexpressing AQP-  
17 1. (Q) Box plot of the directionality of the same cells tracked in (P). (R) Box plot of the  
18 number of transfected cells (pMES and AQP-1 FL) in the neural crest stream 16 hours  
19 after transfection, n=8 pMES embryos, n=10 AQP-1 FL embryos. (S) Representative  
20 tracks of neural crest cells transfected with Gap43-YFP (black) and AQP-1 FL (red). FL,  
21 full length; OV, otic vesicle; ba, branchial arch; AZA, Acetazolamide; ctrl, control; MO,  
22 morpholino.

23

1 **Figure 4: Identification and tracking of in vivo neural crest filopodia reveals AQP-**  
2 **1 expression changes the length, number, growth rate and survival.** (A) Front of r4  
3 stream of neural crest cells of a pMES control (red) and Gap43-mTurquoise2 (green)  
4 labeled HH13 embryo. (B) mTurquoise2 label of individual cell and (C) masked image of  
5 cell for filopodia identification. (D) Each identified filopodium of a single time point for a  
6 cell marked in different colors. (E) Schematic of filopodium identification if filopodia are  
7 bifurcated; one tip is the main filopodia and the branch constitutes a second filopodium  
8 of shorter length. (F) Box plots showing no significant change in filopodia length when  
9 AQP-1 is overexpressed but shorter filopodia when AQP-1 is knocked down by  
10 morpholino. (G) Box plot of the number of filopodia per cell showing a reduction in  
11 number if AQP-1 expression is altered. (H) Percent change in filopodial length from  
12 time point to time point for Control, AQP-1 FL and AQP-1 MO cells. AQP-1  
13 overexpression reduces the rate of filopodial growth or retraction but knock down  
14 increases only the retraction rate. (I) Survival function for filopodia under three  
15 conditions. The probability of a filopodium in a cell overexpressing AQP-1 is much  
16 higher than Control. AQP-1 knock down reduces the survival probability of a filopodium.  
17 (J) Representative mTurquoise2 membrane labeled cells in vivo. All Bars = 20  $\mu$ m.

18

19 **Figure 5: AQP-1 influences focal adhesions and ECM degradation.** (A) Integrated  
20 pathway analysis displaying developmentally relevant signaling pathways affected by  
21 overexpression of AQP-1. (B) Genes associated with ECM GO term that were  
22 significantly up- (red) or down-regulated (blue) in response to overexpression of AQP-1.  
23 (C) Colocalization of pFAK (cyan), AQP-1 (magenta) and EphB3 (green) protein

1 expression in migrating neural crest cells (HNK-1, red) in vivo. Bar=2 um. (D) High  
2 resolution image of neural crest cells (HNK-1, yellow) in vitro transfected with pMES or  
3 AQP-1 FL (red) showing pFAK and integrinB1 expression (white). Bar=5 um. Box plot of  
4 the number of pFAK spots detected in neural crest cells transfected with pMES or AQP-  
5 1 FL, n=10 and 12 respectively. Box plot of the number of integrinB1 spots detected in  
6 neural crest cells transfected with pMES or AQP-1 FL, n=10 and 11 respectively. (E)  
7 Quantification of in gel zymography using AQP-1 and MMP inhibitors, showing 27% and  
8 17% of MMP activity respectively, n=39 neural tubes each for AZA and control, n=32  
9 neural tubes each for GM6001 and control. (F) In vitro degradation assay. Chambered  
10 slides were coated with Cy3-labeled gelatin (orange). Neural tubes transfected with  
11 pMES or AQP-1 FL (GFP) were plated onto the gelatin and incubated for 40 hours. No  
12 neural tubes were used as baseline control. (G) Box plot of the average intensity of  
13 Cy3-labeled gelatin after 40 hours of incubation with no neural crest, pMES transfected  
14 neural crest or AQP-1 FL transfected neural crest, n=15 40x images analyzed per  
15 condition from n=3 replicates each.

16

17 **Figure 6: AQP-1 interacts with EphB receptors and is involved in neural crest cell**  
18 **directionality.** (A) RNAscope of lead r4 neural crest cells in vivo, HNK-1 signal outlined  
19 in white and showing transcripts for *AQP-1* (green). Bar=5 um. (B) RNAscope of same  
20 cells in (a) with *AQP-1* (green), *EphB1* (cyan) and *EphB3* (purple). (C) Bar graph of  
21 number of cells per embryo expressing different mRNA combinations. (D) Bar graph of  
22 average number of transcripts of each gene in cells with or without *AQP-1* mRNA. (E-H)  
23 Protein expression of AQP-1 (E), EphB1/B3 (F) and HNK-1 (G) in migrating neural crest

1 cells (H) at HH13. Bar=5 um. (I) Schematic representation of in vitro assay quantified in  
2 (J). (J) Box plot of the directionality of neural crest cells responding to branchial arch 2  
3 tissue in vitro, n=18 untransfected cells, n=25 AQP-1 FL cells, n=42 pMES cells.

4

5 **Figure 7: Computer simulations predicts that increased speed, filopodia**  
6 **stabilization and ECM degradation enhance cell invasion.** (A) Model parameters for  
7 various experimental and hypothetical scenarios. (B) Schematic representations of chain  
8 migration where followers (yellow) within a certain distance of each other all adopt the  
9 direction of movement of the leader (black), tunnel movement where the tunnel (blue)  
10 forged by a leader guides followers that enter the tunnel to move along the tunnel and  
11 chain and tunnel movement where a leader can guide followers both via the tunnel it has  
12 created and by chain movement. (C, E-G) Distribution of cells along the domain for  
13 different models, average of 10 simulations at t=24 hours. (D) Boxplots of fractions of  
14 follower cells not in chains (also not in tunnels in Model 10 and Model 11) at t=24 hours.  
15 Results are averaged over 10 simulations. For each model, the red line indicates the  
16 median, and the bottom and top edges of the box indicate the 25th and 75th percentiles,  
17 respectively. The dotted lines extend to the most extreme data points not considered  
18 outliers, and the outliers are plotted individually as red dots. M - Model. (H) Snapshots  
19 from three selected models at t=24 hours. Black circles – leader cells, yellow circles –  
20 follower cells, blue circles – positions of one of the leaders that form a tunnel, c –  
21 concentration of chemoattractant (VEGF).

22



1 **Supplemental Figure 1.** (A) No probes control for RNAscope experiment. (B)  
2 Quantification of AQP-1 RNA expression in chick embryonic fibroblasts (CEF), chick  
3 liver hepatocellular carcinoma (LMH) and LMH transfected with AQP-1 FL. (C)  
4 Quantification of AQP-1 RNA expression in LMH cells after mock transfection, pMES  
5 transfection and AQP-1 FL transfection. (D) Box plot of the Speed (microns/hr) of neural  
6 crest cells, transfected with pMES control vector (black, n= 27 cells from n=9 neural  
7 tube explants), non-transfected but in the same cultures as pMES (blue, n=26 cells) and  
8 transfected with AQP-1 FL in different cultures but prepared and imaged the same days  
9 as controls (red, n=33 cells from n=10 neural tube explants). (E) Box plot of the  
10 distance migrated by neural crest cells after mesodermal injections of AZA (red) and the  
11 distance migrated by neural crest cells on the control sides of the same embryos  
12 (black), n=6 embryos. (F) Box plot of the percentage of neural crest cells that migrate  
13 into the branchial arches, n=8 embryos per treatment. (G) The entire zymogram that is  
14 quantified in Figure 5. An image of the ladder (left) was taken prior to development so  
15 that it could be clearly seen. Proteins in these assays do not run exactly the same as  
16 the markers as enzymes in the samples are not reduced while the markers are  
17 (Woessner, 1995). The band size is approximately 62 kD, corresponding to MMP2  
18 (Anderson, 2010).

19

20 **Supplemental Figure 2: Filopodia direction and length with respect to neural**  
21 **crest migratory direction.** (A) Distribution of angles of filopodia for control (black),  
22 AQP-1 FL overexpression vector (green) and the AQP-1 MO (red) labeled cells. Radial  
23 magnitude equals number of filopodia in that direction. (B) Length and direction of the

1 filopodia for cells labeled with control vector, AQP-1 FL overexpression vector or AQP-1  
2 morpholino. Radial magnitude equals length of the filopodia in microns and angle is  
3 with respect to migratory direction. Contrasting colored filopodia are in a 30° window  
4 around the direction of migration. (C) Example neural crest filopodia with direction of  
5 migration indicated. Direction of migration is always set to 0 degrees.

6 **Supplemental Figure 3:** Schematic of a rectangular domain we used to model the  
7 domain on which the neural crest cells migrate (black circles). They enter the domain  
8 from the neural tube ( $x = R$ ). BA2 denotes branchial arch 2.

9

10 **Supplemental Table 1:** Genes that are differentially expressed between pMES  
11 (control) and AQP-1 FL. (excel document, not attached)

12

13 **Supplemental Table 2: Model parameters used in the simulations provided in the**  
14 **results section.**

15

16 **Supplemental Movie 1: Cranial neural crest cell migratory behaviors are altered in**  
17 **vitro after AQP-1 manipulation.** (top) Control migrating neural crest cells exposed to  
18 DMSO. (middle) AQP-1 was inhibited by adding Acetazolamide (AZA) to the media.  
19 AZA was solubilized in DMSO. (bottom) AQP-1 was overexpressed by transfection of  
20 AQP-1 full length construct (green cells). Cranial neural tube explants are shown on the  
21 left-hand side of each panel. Time intervals between images ranged from 2.5 to 4

1 minutes and frame speed was adjusted so that each time-lapse was 8 hours in duration.

2 Scale bar= 30 um.

3

4 **Supplemental Movie 2: Cranial neural crest cell migratory behaviors are altered**

5 **in vivo after AQP-1 manipulation.** (Left) Premigratory neural crest cells were

6 transfected with Gap43-YFP/H2B mCherry (control). (Right) AQP-1 full length/H2B

7 mCherry. Z-stacks were collected every 5 minutes and approximately 6 hours is shown.

8 Scale bar= 20 um.

9

10 **Supplemental Movie 3: Fast confocal imaging reveals changes in neural crest cell**

11 **filopodial dynamics after AQP-1 manipulation.** Projected images from spinning disk

12 time-lapse microscopy of migrating lead neural crest cells in whole embryo culture

13 electroporated with either (top) pMES control, (middle) AQP-1 FL or (bottom) AQP-1

14 Morpholino (MO). Each movie sequence shows the cell membrane label (Gap43-

15 mTurquoise2) to highlight the cell protrusion dynamics. Images were collected in 30

16 second intervals and shown here for approximately 11 min.

17

18 **Supplemental Movie 4: Cranial neural crest cell directionality is altered after AQP-**

19 **1 manipulation.** Premigratory neural crest were transfected with pMES (control) or

20 AQP-1 FL and neural tubes were plated in the presence of branchial arch 2 (ba2) tissue

21 as a source of known endogenous chemoattraction. Images were collected every 5

1 minutes and a total of approximately 18 hours of elapsed time is shown. Scale bar= 50  
2 um.

3

4 **Supplemental Movie 5: Computer model simulations of cranial neural crest cell**  
5 **migration with AQP-1 manipulation.** (top) Control migration is modeled by normal cell  
6 speed and unstable filopodia. (middle) AQP-1 loss-of-function is modeled by reduced  
7 cell speed and reduced number of cell filopodia. (bottom) AQP-1 gain-of-function is  
8 modeled by increased cell speed, stable cell filopodia and tunneling. Each simulation is  
9 run on a 2D migratory domain.



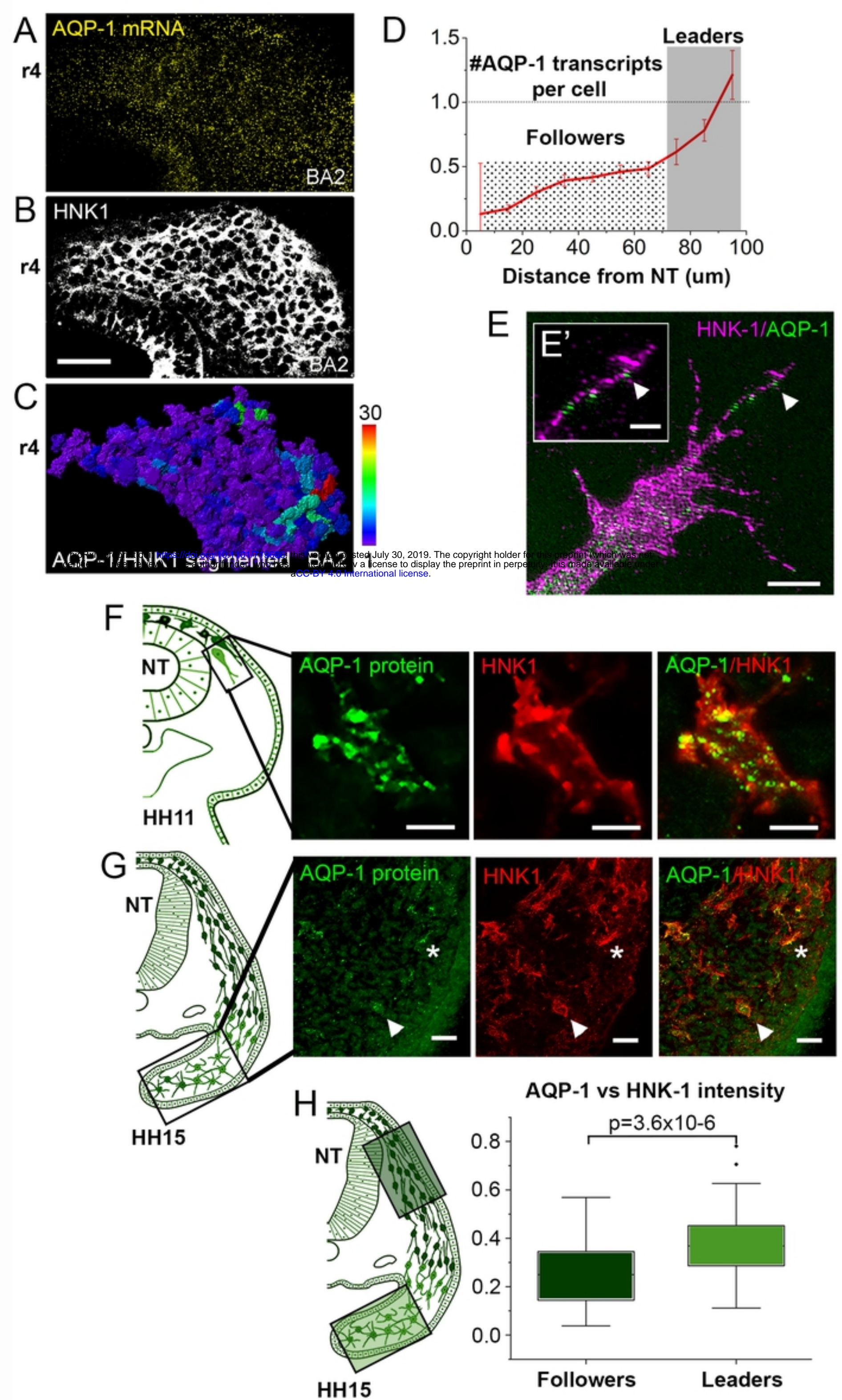
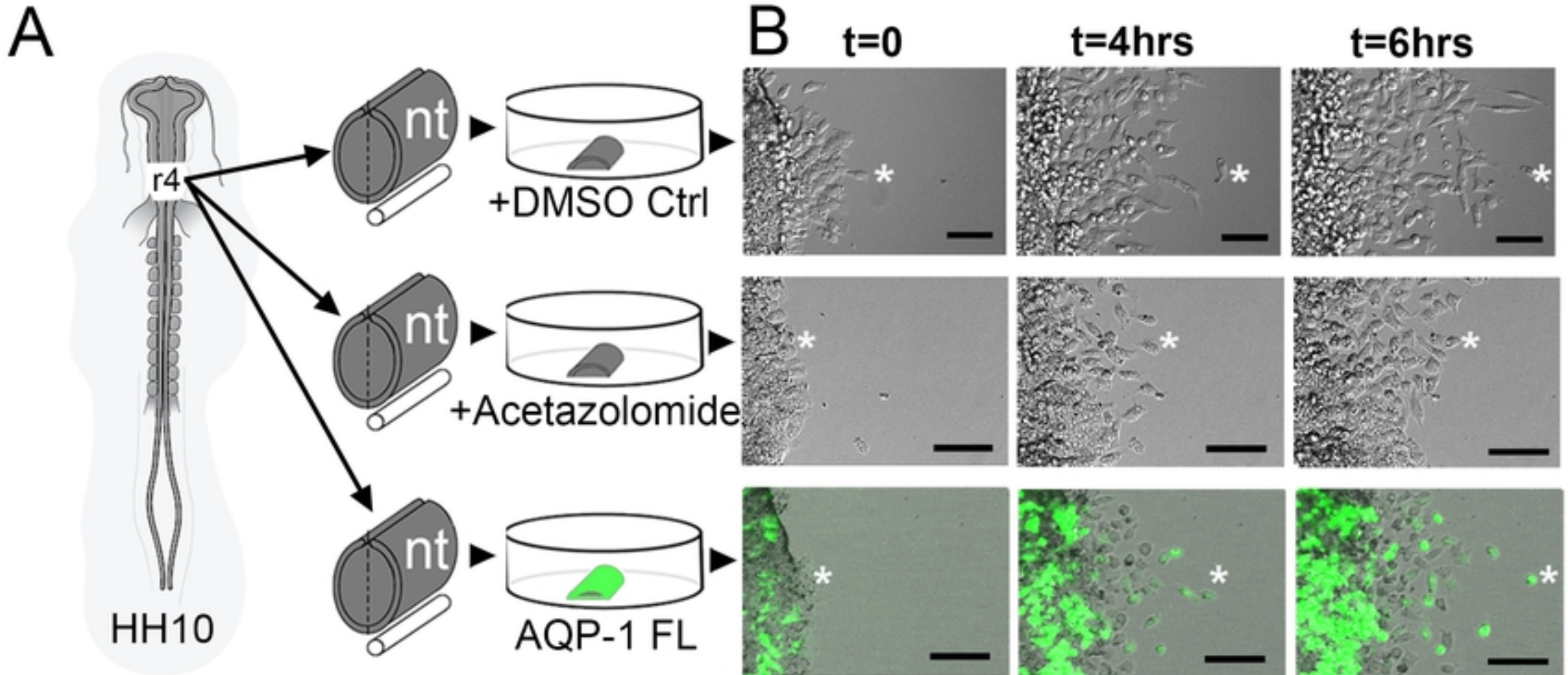


Figure 1





**C** bioRxiv preprint doi: <https://doi.org/10.1101/719666>; this version posted July 30, 2019. The copyright holder for this preprint (which was not certified by peer review) is the author/funder, who has granted bioRxiv a license to display the preprint in perpetuity. It is made available under aCC-BY 4.0 International license.

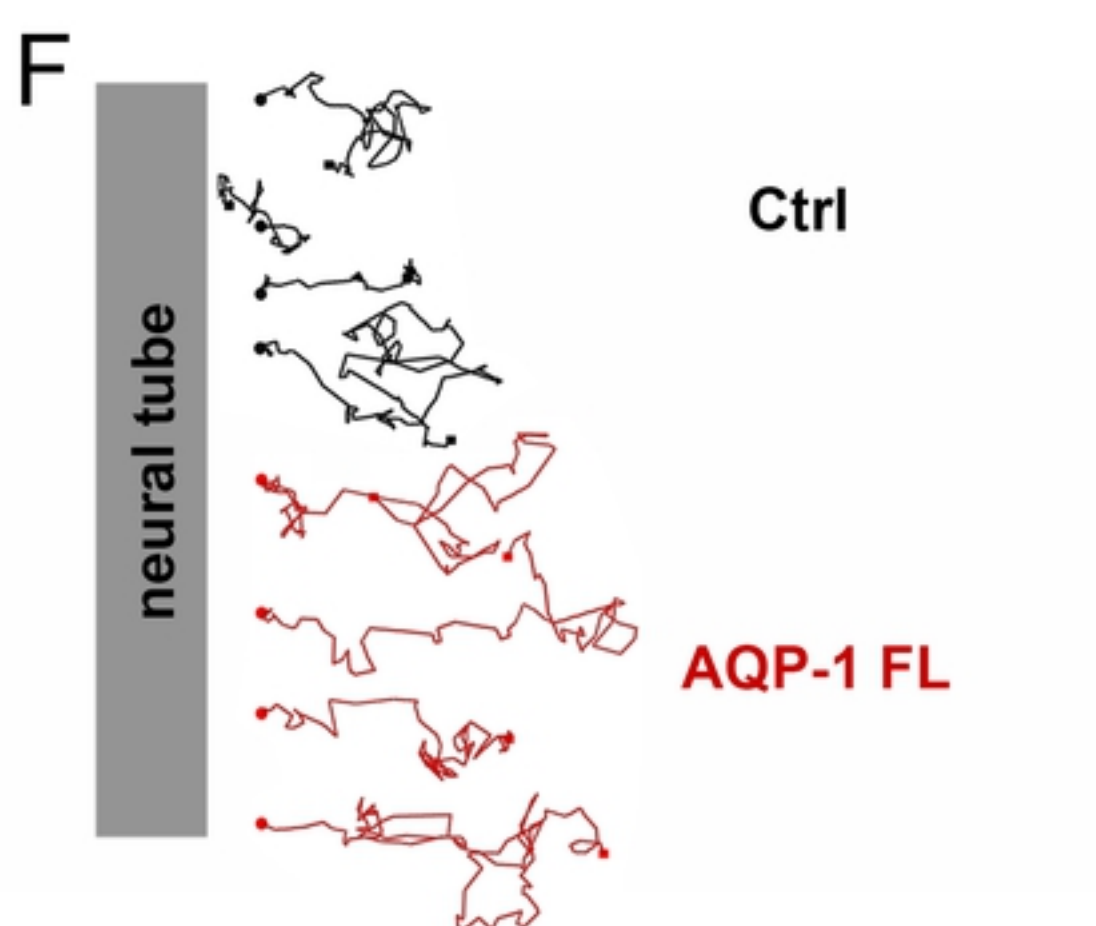
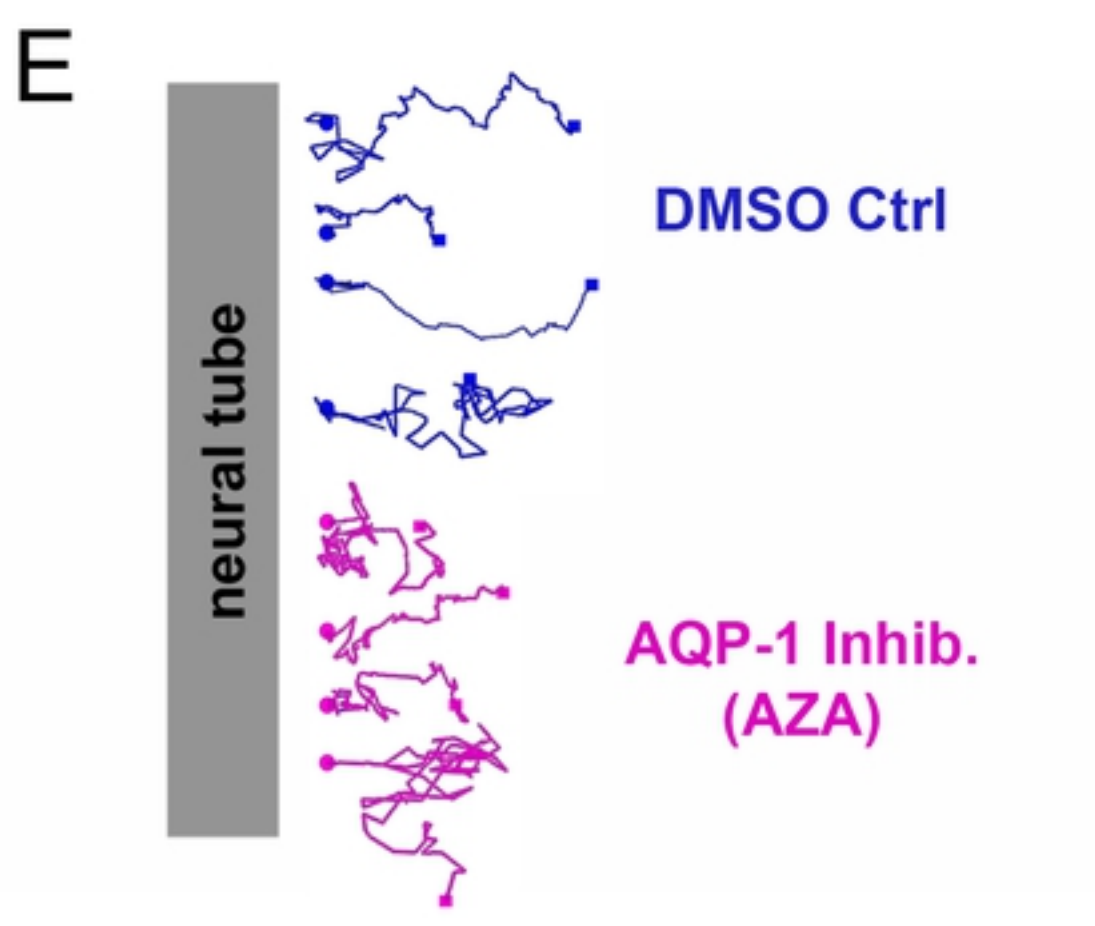
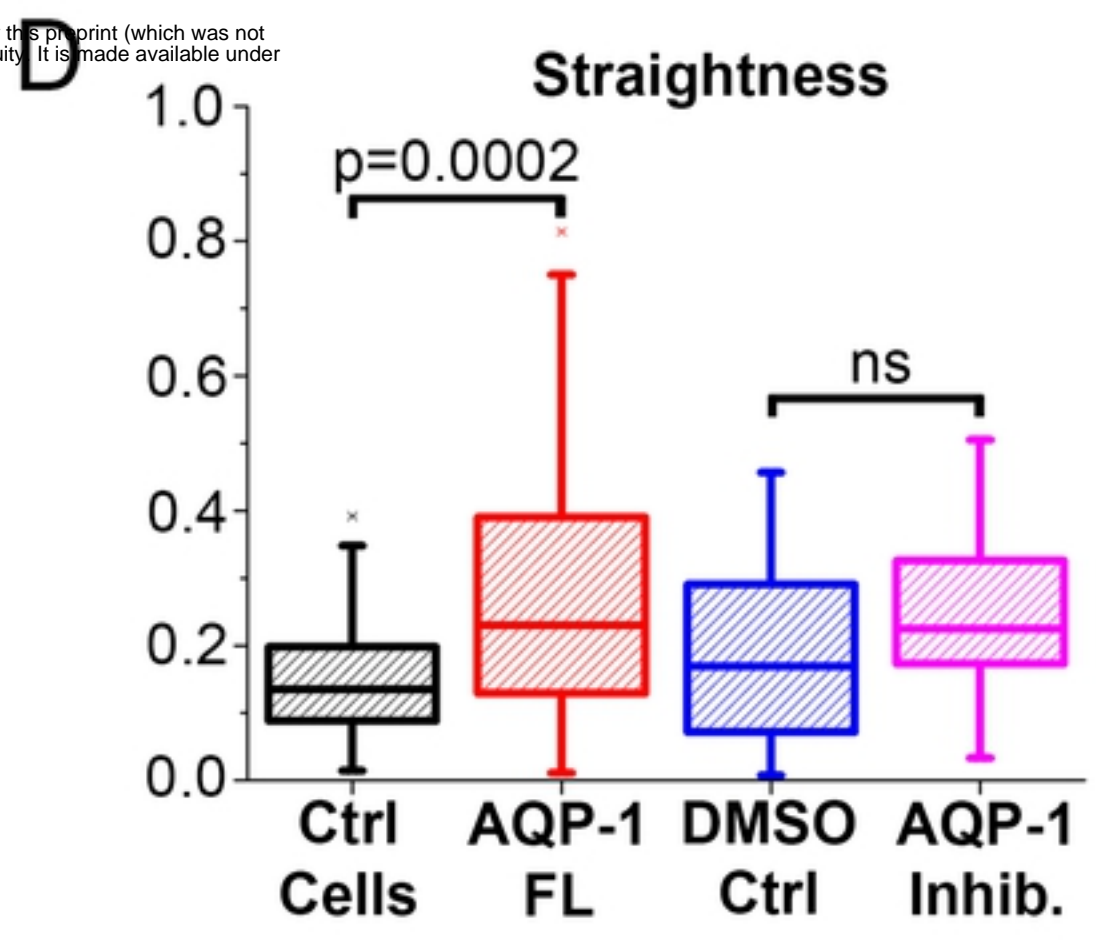
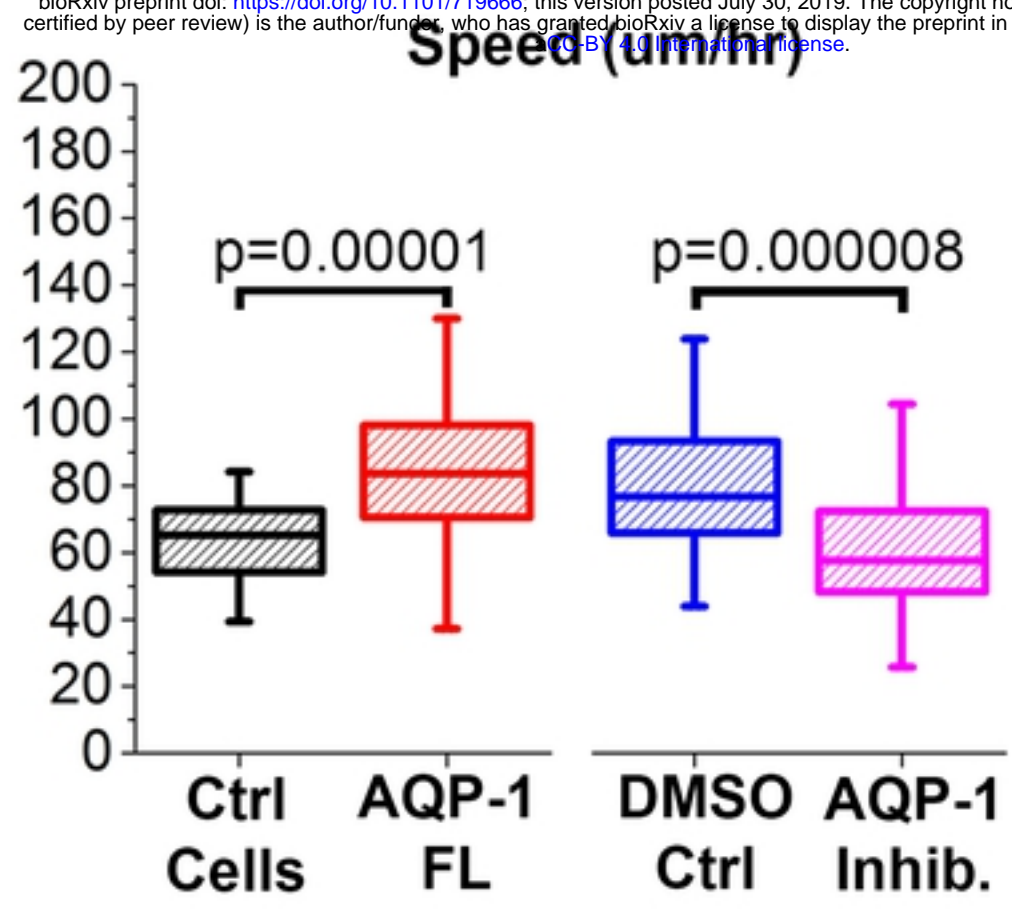


Figure 2



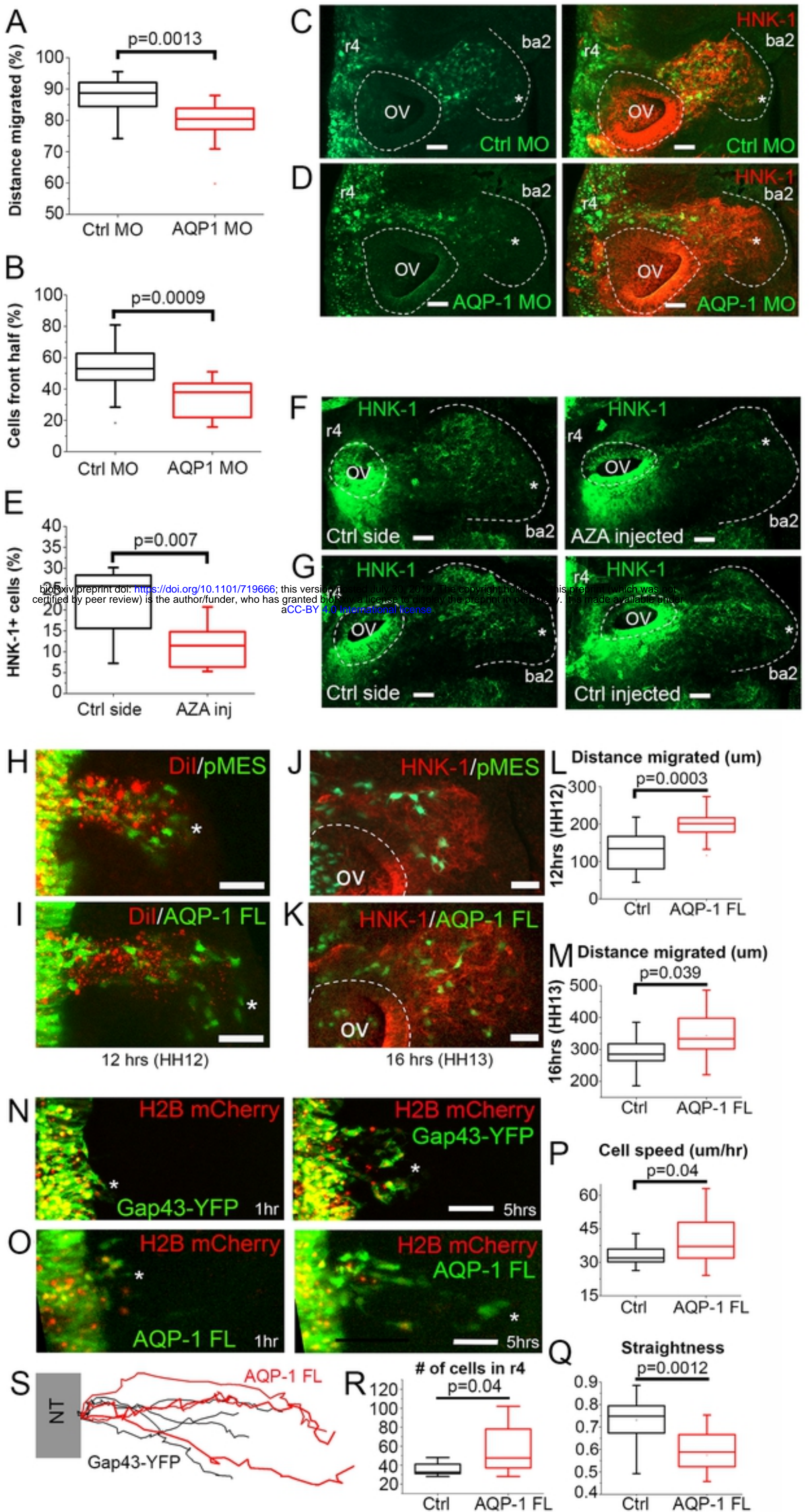


Figure 3



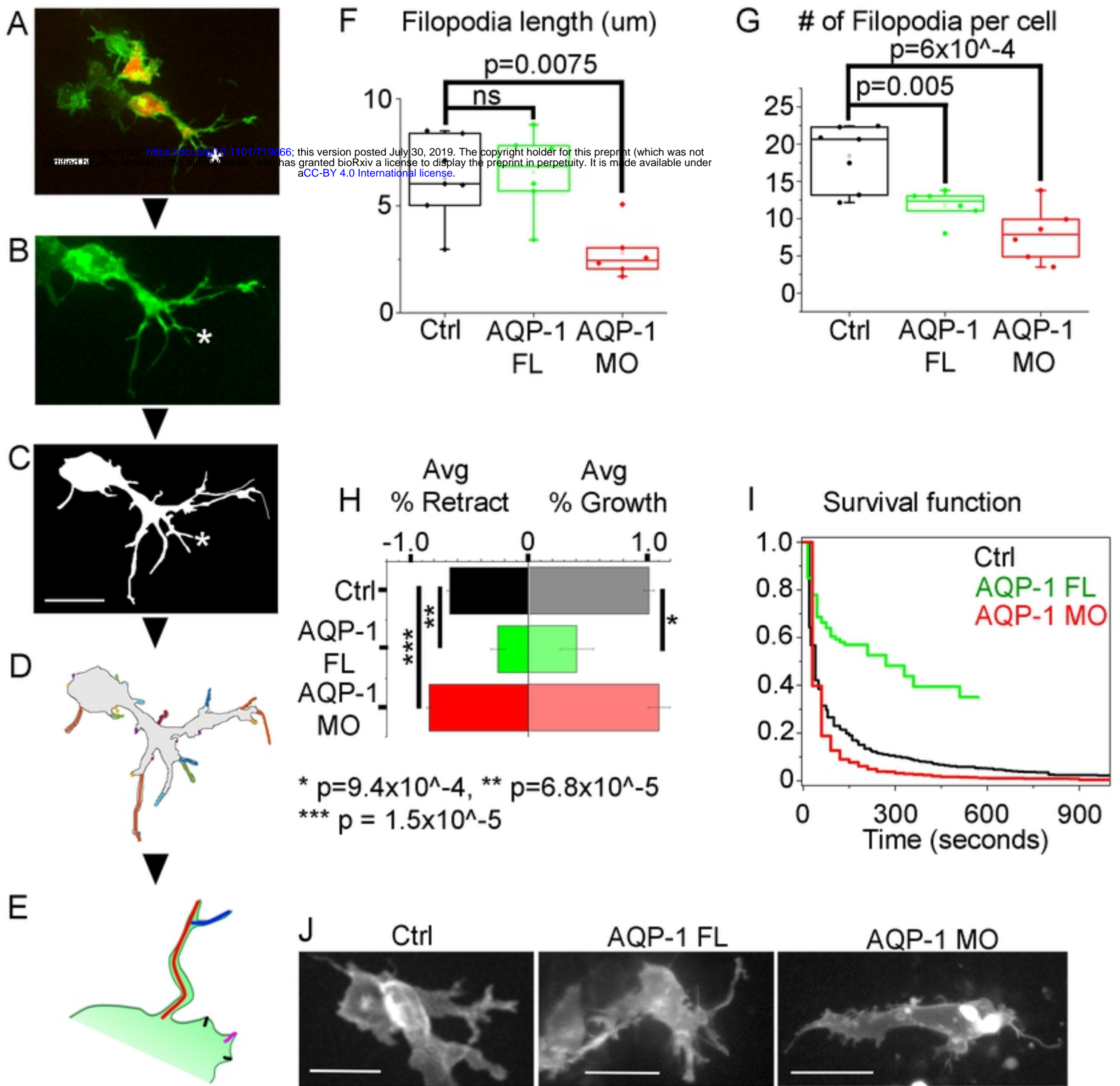


Figure 4



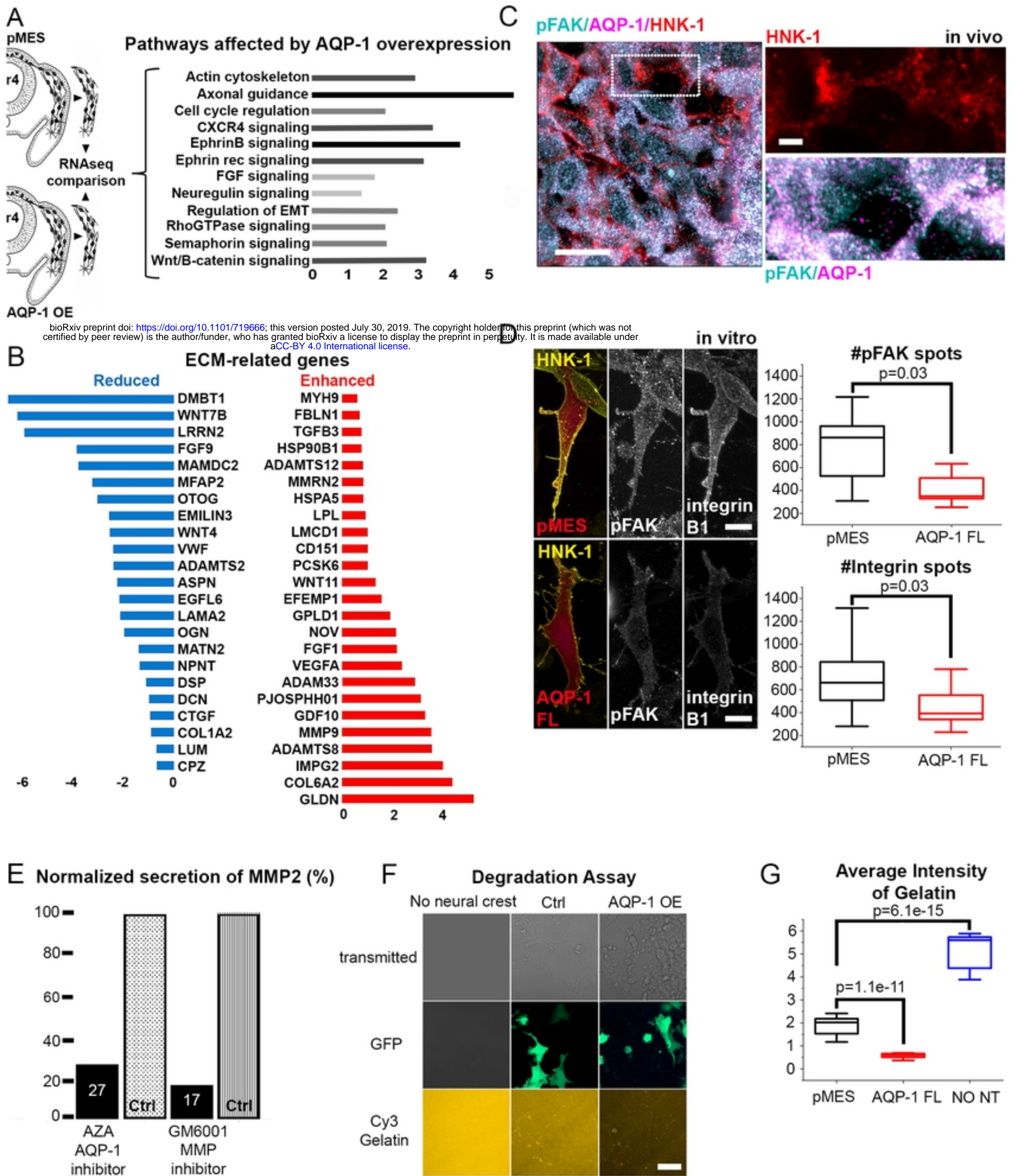


Figure 5



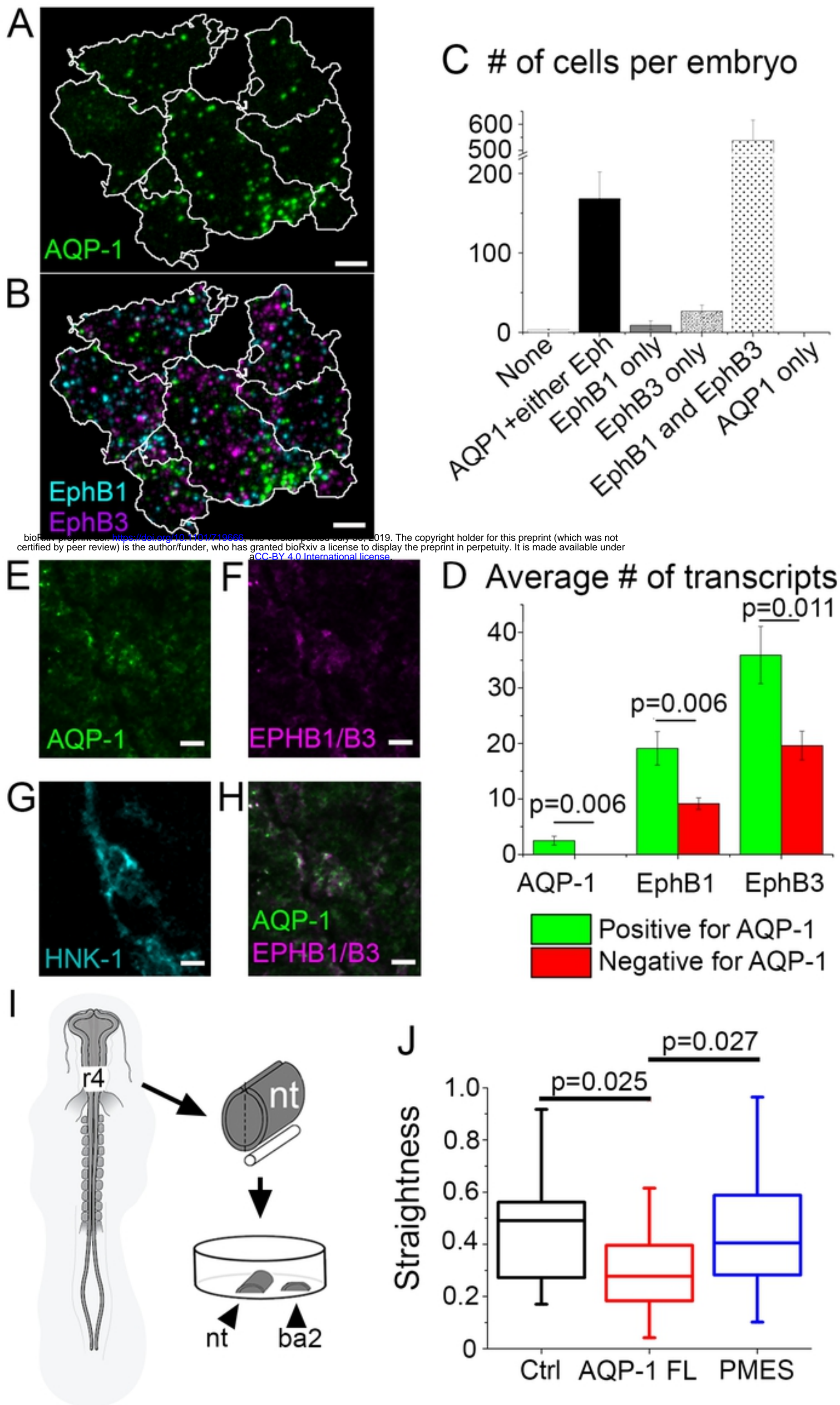
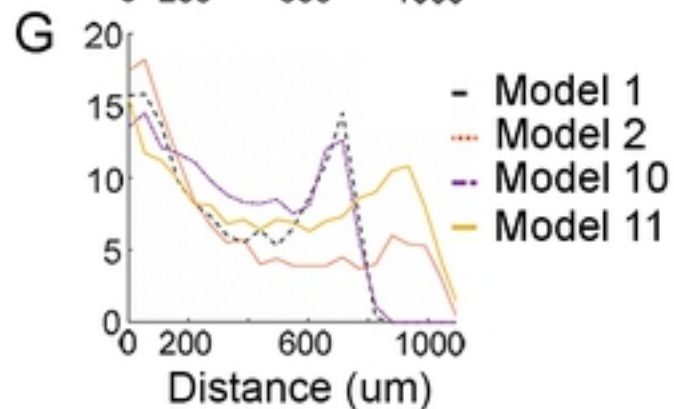
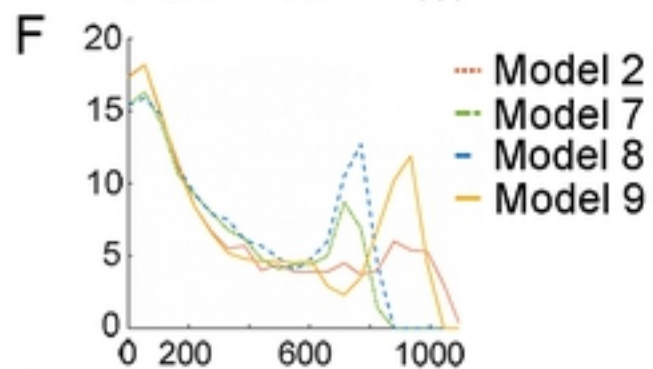
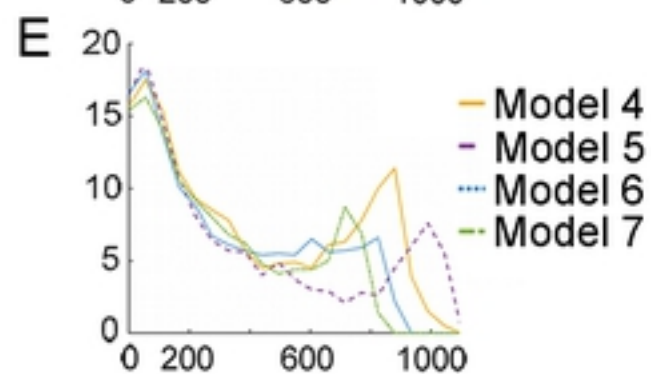
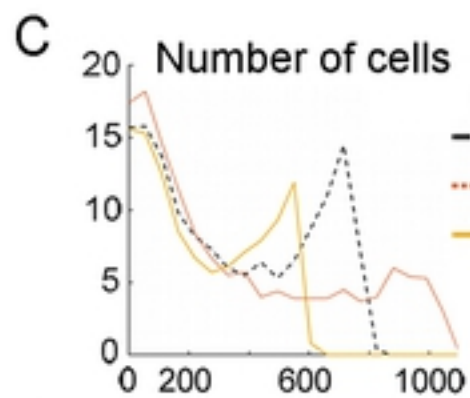
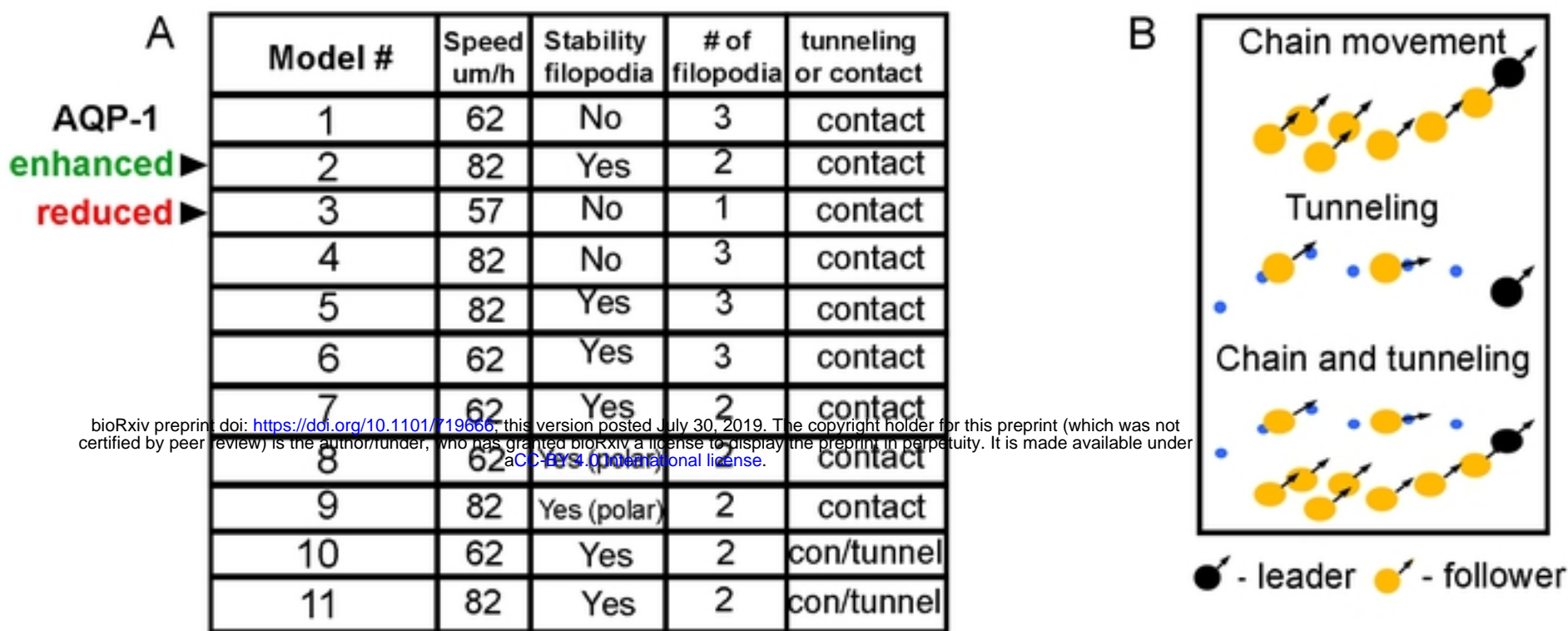


Figure 6



**D** % Follower cells not in chains vs Model Number

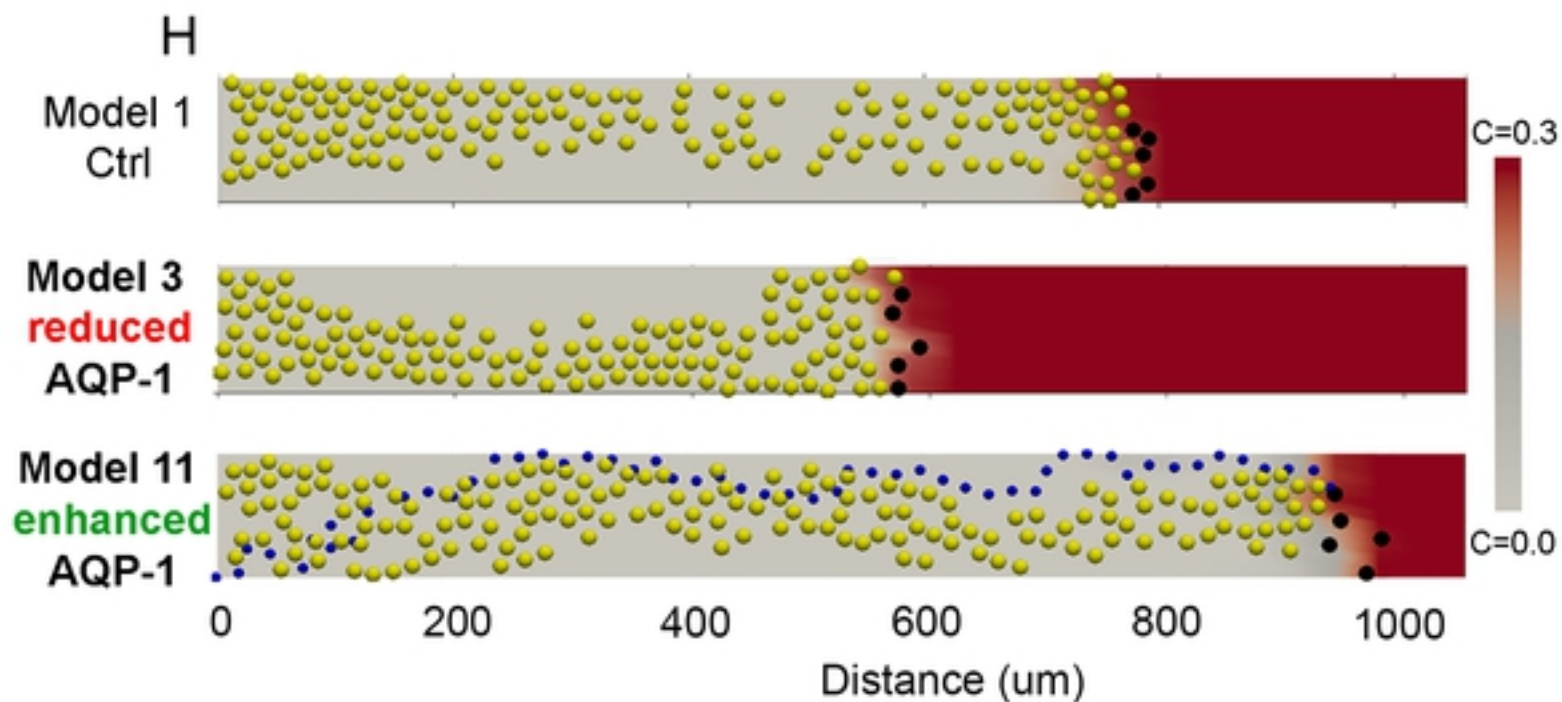
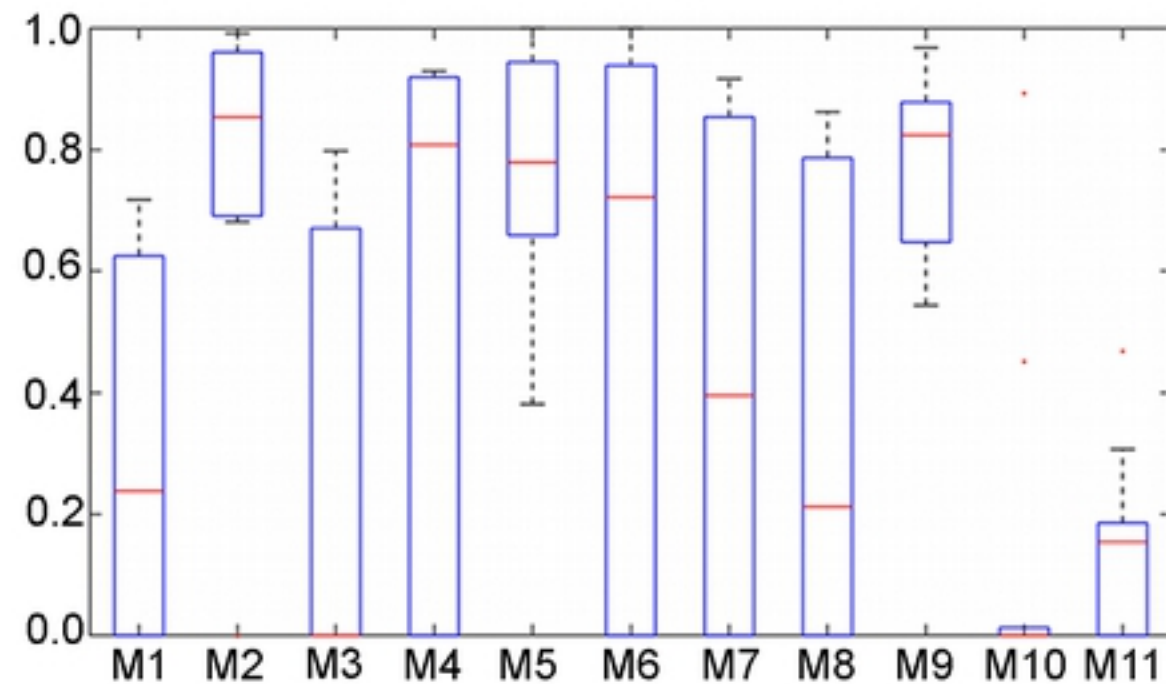


Figure 7